# Theoretical Guarantees and Training Dynamics of Contrastive Learning: How Misaligned Data Influence Feature Purity

**Jiawei Sun** SUNJ11@RPI.EDU
*Rensselaer Polytechnic Institute, Troy, NY, USA*

**Shuai Zhang** SHUAI.ZHANG@NJIT.EDU
*New Jersey Institute of Technology, Newark, NJ, USA*

**Hongkang Li** LIHK@SEAS.UPENN.EDU
*University of Pennsylvania, Philadelphia, PA, USA*

**Meng Wang** WANGM7@RPI.EDU
*Rensselaer Polytechnic Institute, Troy, NY, USA*

## Abstract

Contrastive learning is a powerful framework for learning discriminative representations from image-text pairs. Despite its success, its theoretical foundations, especially when the image-text pair exhibits misalignment, remain underexplored. This paper provides the first theoretical analysis of contrastive learning under data misalignment, proving how the ground-truth modality-paired features are amplified while spurious features are suppressed through the training dynamics analysis. Specifically, we study two nonlinear encoders trained jointly with a contrastive loss and demonstrate that noisy (or misaligned) data pairs result in mixed representations and degrade the model's generalization ability. In contrast, recaptioning and filtering improve the data alignment, which in turn purifies the features learned by neurons and subsequently enhances generalization. Our analysis identifies feature purity as a key factor in the success of contrastive learning and offers insights into how data quality and training procedures impact representation learning and downstream generalization. Theoretical insights are supported by experiments on standard benchmarks.

**Keywords:** Contrastive Learning, Training Dynamics, Feature Learning, Generalization Guarantees

## 1. Introduction

Vision-language models (VLMs) achieve strong results in tasks like image captioning and retrieval by contrastively aligning image-text pairs. Leading methods such as CLIP [16] and SimVLM [23] train dual encoders on large-scale web data, pulling matched pairs closer in a shared embedding space. These models are highly effective in zero-shot settings without task-specific tuning. However, web-sourced captions often include irrelevant or spurious content, weakening cross-modal alignment. For instance, [15] highlights an image of a Mercedes-Benz paired with a caption describing its price and leather seats—details not visually inferable from the image. Such misalignments degrade representation quality and generalization. To address this, many works [2, 6, 8, 15, 17, 20, 21] use text generation models to rewrite captions during training. Methods like LaCLIP [6] and BLIP [12] improve both caption quality and diversity, leading to better model performance.

Despite empirical success, the theory behind VLM pretraining and recaptioning remains underdeveloped. Key open questions include:

How do contrastively trained VLMs learn aligned features and enable zero-shot inference? How does text recaptioning on noisy image-text pairs provably enhance generalization performance?

Prior theoretical studies either assume convergence to optimal solutions [7, 9, 11, 27], or focus on simplified settings—e.g., unimodal or linear models [4, 14, 24]. None address training dynamics under misalignment or the effect of recaptioned text on feature quality.

**Contributions.** We present the first theoretical analysis of how text recaptioning improves zero-shot generalization in VLMs under modality misalignment. First, we analyze the training dynamics of multimodal contrastive learning with two ReLU networks, extending prior results beyond linear or unimodal settings. Second, we formalize a misalignment model in which spurious or missing features entangle the learned representations and degrade generalization. Third, we prove that recaptioning and filtering reduce spurious correlations and enhance semantic relevance, leading to improved representations and out-of-domain performance.

## 2. Problem Formulation and Algorithm

VLMs are pre-trained on large-scale web datasets of paired images and texts using dual encoders: an image encoder $f_{\mathbf{W}}$ and a text encoder $h_{\mathbf{V}}$, parameterized by weights $\mathbf{W}$ and $\mathbf{V}$. Contrastive learning pulls positive pairs close and pushes apart negative ones. Let $S$ be the index set of image-text pairs $(x_p, y_p)$. A pair $(x_p, y_p)$ is positive, while $(x_p, y_n)$ with $p \neq n$ is negative. Training minimizes a spectral loss over these pairs.

$$L(f,h) = \sum_{p\in S}\left[-\langle f(x_p), h(y_p)\rangle + \sum_{n\in S\setminus\{p\}} \frac{\left(\langle f(x_n), h(y_p)\rangle\right)^2}{2\tau} + \sum_{n\in S\setminus\{p\}} \frac{\left(\langle f(x_p), h(y_n)\rangle\right)^2}{2\tau}\right] \tag{1}$$

where the hyper-parameter $\tau > 0$ is referred as the temperature.

### 2.1. Training Framework

Let $S = S_h \cup S_w$ include human-annotated high-quality image-text pairs with indices in $S_h$ and noisy web low-quality dataset with indices in $S_w$. Due to the inherently noisy nature of web data, the learned embeddings from (1) may be suboptimal. To address this, many methods [6, 12] use rewritten text to enhance image-text pair quality and diversity. Though implementations differ, most follow a similar four-stage framework:

(S1) **Image-text contrastive pre-training (ITCP) on raw data:** The image encoder $f$ and text encoder $h$ are trained using the image-text pairs $\{(x_p, y_p)\}_{p\in S}$ by minimizing the contrastive loss as in (1). Let $\overline{\mathbf{W}}$ and $\overline{\mathbf{V}}$ denote the learned weights in $f$ and $h$. We then estimate the image and text embeddings of $(x_p, y_p)$ by $z'_{x_p} = f_{\overline{\mathbf{W}}}(x_p)$ and $z'_{y_p} = h_{\overline{\mathbf{V}}}(y_p)$. Due to the low-quality data in $S_w$ when training the encoders, these estimations might not be accurate.

(S2) **Generating text captions:** The high-quality data pairs in $S_h$ are used to finetune an image-grounded text decoder $G$, which maps an image $x_p$ to text through $G(x_p)$. Then, the learned $G$ is applied to every image $x_p$ in $S_w$ to generate a synthetic caption $\hat{y}_p = G(x_p)$. Next, the estimated text embedding of $\hat{y}_p$ is computed as $\hat{z}_{y_p} = h_{\overline{\mathbf{V}}}(\hat{y}_p) = h_{\overline{\mathbf{V}}}(G(x_p))$, where $\overline{\mathbf{V}}$ represents the weights of $h$ learned from Stage S1.

(S3) **Filtering:** For every $(x_p, y_p) \in S_w$, we compute the cosine similarity between the image embedding $z'_{x_p}$ and the text embeddings of the original caption $z'_{y_p}$ and the synthetic caption $\hat{z}_{y_p}$. If $(z'_{x_p}, \hat{z}_{y_p})$ yields higher similarity than $(z'_{x_p}, z'_{y_p})$, we replace $(x_p, y_p)$ with $(x_p, \hat{y}_p)$. Let $\tilde{S}_w$ denote the index set of selected data pairs. By filtering out noisy captions in $S_w$ and replacing them with better-aligned synthetic ones, $\tilde{S}_w$ forms a cleaner dataset for training.

(S4) **ITCP on filtered data:** The image encoder $f$ and text encoder $h$ are trained by minimizing the contrastive loss in (1), repeating the procedure from Stage 1 (S1) with the only difference being that the original dataset $S$ is replaced by $\tilde{S} = S_h \cup \tilde{S}_w$. The resulting loss is denoted by $\tilde{L}(f, h)$. Let $\widetilde{\mathbf{W}}$ and $\widetilde{\mathbf{V}}$ denote the resulting learned weights. $f_{\widetilde{\mathbf{W}}}$ and $g_{\widetilde{\mathbf{V}}}$ can produce improved embeddings compared with $f_{\overline{\mathbf{W}}}$ and $g_{\overline{\mathbf{V}}}$.

### 2.2. Downstream Tasks

As a demonstration of the performance of the learned model $(f_{\widetilde{\mathbf{W}}}, g_{\widetilde{\mathbf{V}}})$, we consider a downstream image classification task in a zero-shot setting. We consider a $K$-classification problem for any constant $K \geq 2$. Each class label is associated with a given text prompt $y_k$, where $k \in [K]$. For any image $x$ with its ground-truth label $l_x \in [K]$, the zero-shot predicted label by the pre-trained models $(f_{\widetilde{\mathbf{W}}}, g_{\widetilde{\mathbf{V}}})$ is computed as $\arg\max_{k \in [K]} \langle f_{\widetilde{\mathbf{W}}}(x), g_{\widetilde{\mathbf{V}}}(y_k) \rangle$. This approach follows the typical setting of zero-shot classification takes [4, 10, 12].

## 3. Technical Assumptions and Setups

We introduce a set of assumptions that are either derived conceptually from the real data distribution or follow existing approaches in contrastive learning theory.

### 3.1. Backbone of the Encoders

We use a two-layer neural network with ReLU activation functions as the image and text encoder, respectively. Formally, we have

**Definition 1** *The image encoder $f_{\mathbf{W}} : \mathbb{R}^{d_1} \to \mathbb{R}^m$ and text encoder $h_{\mathbf{V}} : \mathbb{R}^{d_1} \to \mathbb{R}^m$ is*

$$f(x) = (f_1(x), \ldots, f_m(x))^\top \in \mathbb{R}^m, \quad \textit{with} \quad f_i(x) = \sigma(\langle w_i, x \rangle - b_i) - \sigma(-\langle w_i, x \rangle - b_i), \tag{2}$$

$$h(y) = (h_1(y), \ldots, h_m(y))^\top \in \mathbb{R}^m, \quad \textit{with} \quad h_i(y) = \sigma(\langle v_i, y \rangle - b_i) - \sigma(-\langle v_i, y \rangle - b_i), \tag{3}$$

*where $\sigma$ is ReLU function, and $\mathbf{W} = [w_1, w_2, \ldots, w_m]^\top$, $\mathbf{V} = [v_1, v_2, \ldots, v_m]^\top \in \mathbb{R}^{m \times d_1}$.*

### 3.2. Data Model for ITCP

**Assumption 1 (Sparse coding model for image-text pairs)** *Each image-text pair $(x_p, y_p)$, $p \in S$, is generated i.i.d. from the following sparse coding form:*

$$x_p = \mathbf{M} z_{x_p} + \xi_{x_p}, \quad y_p = \mathbf{H} z_{y_p} + \xi_{y_p}, \tag{4}$$

*where $x_p, y_p \in \mathbb{R}^{d_1}$, $z_{x_p}, z_{y_p} \in \mathbb{R}^d$, and $d_1 = \mathrm{poly}(d)$. We assume:*

*(a) Image dictionary: $\mathbf{M} = [\mathbf{M}_1, \ldots, \mathbf{M}_d] \in \mathbb{R}^{d_1 \times d}$ is column-orthonormal.*

*(b) Text dictionary: $\mathbf{H} = [\mathbf{H}_1, \ldots, \mathbf{H}_d] \in \mathbb{R}^{d_1 \times d}$ is column-orthonormal.*

*(c) Additive noise: $\xi_{x_p}, \xi_{y_p} \sim \mathcal{N}(0, \sigma_\xi^2 \mathbf{I}_{d_1})$ with $\omega(1/d_1) \leq \sigma_\xi^2 \leq O\big(\sqrt{\log d / d^{1+c_0}}\big)$.*

*(d) Sparse latent vector: $z_{x_p} = (z_{x_p}^1, \ldots, z_{x_p}^d)$ with $z_{x_p}^j \in \{0, \pm 1\}$, where $|z_{x_p}^j| \sim$ Bernoulli$(C_z/d)$.*

We introduce Assumptions 2 and 3 to capture the characteristics of the dataset $S = S_h \cup S_w$. Notably, high-quality pairs in $S_h$ may be significantly fewer than low-quality pairs in $S_w$, with $|S_h| = \Theta(d^2)$ and $|S_w| = \mathrm{poly}(d) \gg \omega(d^2)$. For high-quality data $S_h$, we assume learnable latent feature, consistent with the common assumption in prior work [4] that focuses exclusively on such data in contrastive learning.

**Assumption 2 (High-quality image-text pairs)** *Every high-quality image-text pair $(x_p, y_p)$ with $p \in S_h$ shares the learnable latent feature, i.e., $z_{x_p} = z_{y_p}$, where $z_{x_p}$ and $z_{y_p}$ denote the shared feature representations underlying the image and text, respectively.*

Compared to high-quality pairs in $S_h$, low-quality pairs in $S_w$ suffer from modality misalignment, modeled as either spurious image-text correlations or missing text descriptions.

**Assumption 3 (Low-quality image-text pairs)** *There exists a constant $C_s \in (\omega(\frac{1}{\log d}), 1/2)$ such that for every low-quality pair $(x_p, y_p)$ in $S_w$ and every image feature $\mathbf{M}_j$ ($j \in [d]$) in $x_p$, we have*

$$\Pr\left(z_{y_p}^{j'} = z_{x_p}^{j} \mid |z_{x_p}^{j}| = 1\right) = C_s, \quad \Pr\left(z_{y_p}^{j} = 0 \mid |z_{x_p}^{j}| = 1\right) = C_s, \tag{5}$$

*where the first term in (5) is the probability that a text feature $\mathbf{H}_{j'}$ ($j' \neq j$) is spuriously correlated to the image feature $\mathbf{M}_j$, and the second term is the probability that $\mathbf{H}_j$ is missing in the text while the image feature $\mathbf{M}_j$ exists.*

### 3.3. Image-Grounded Text Decoder $G$ in Stage (S2)

Recall that $G$ is employed in Stage (S2) to generate synthetic text captions. In practice, the core idea behind the widely adopted approaches [12, 22, 26] is to train the encoder-decoder model $G$ and leverage the high-quality image-text pairs $S_h$ to improve its performance. In this paper, we consider a simplified form of $G$, given by:

$$G(x_p) = \mathbf{V}^T \sigma(\mathbf{W} x_p), \tag{6}$$

where $\sigma$ denotes the ReLU function. The parameters $\mathbf{W}$ and $\mathbf{V}$ are learned by solving

$$\min_{\mathbf{W},\mathbf{V}} L_C = \sum_{p \in S_h} \frac{1}{2} \left\| \mathbf{V}^T \sigma(\mathbf{W} x_p) - y_p \right\|_2^2, \tag{7}$$

initialized at $\overline{\mathbf{W}}$ and $\overline{\mathbf{V}}$, using SGD with step size $\eta$. Although $G$ in (6) is a conceptual simplification, where $\sigma(\mathbf{W} x_p)$ acts as the encoder and $\mathbf{V}^T$ as the decoder, it serves as a realistic abstraction to illustrate the underlying advantages of synthetic text caption generation.

## 4. Main Results

### 4.1. Feature Purity Improvements in Converged Models via Recaptioned Data

We first characterize the training dynamics and convergence of solving (1) using SGD in Stage S1 and S4 in Sec 2.1. Let $L^*$ and $\tilde{L}^*$ denote the optimal values of the contrastive loss on the raw dataset $S$ and the filtered dataset $\tilde{S}$, respectively. Note that $(\overline{\mathbf{W}}, \overline{\mathbf{V}})$ and $(\widetilde{\mathbf{W}}, \widetilde{\mathbf{V}})$ are the converged weights from contrastive training on $S$ and $\tilde{S}$ in stage S1 and S4, respectively.

**Theorem 2 (Convergence of ITCP)** *Suppose Assumptions 1 to 3 hold. Let the model complexity be $m = d^{1.01}$, initialized at $w_i^{(0)}, v_i^{(0)} \sim \mathcal{N}(0, \sigma_0^2 \mathbf{I}_{d_1})$, where $\sigma_0^2 = \Theta\left(\frac{1}{d_1 poly(d)}\right)$. After $T = \Theta\left(d^2 \log d\right)$ iterations with batch size $B = \Omega(d)$ and $\eta = O(1)$, the returned weights achieve a loss that is sufficiently close to the optimal loss in Stage S1 and Stage S4, respectively, i.e.,*

$$(L(f_{\overline{\mathbf{W}}}, h_{\overline{\mathbf{V}}}) - L^*)/\left|L^*\right| \leq o(1), \quad (\tilde{L}(f_{\widetilde{\mathbf{W}}}, h_{\widetilde{\mathbf{V}}}) - \tilde{L}^*)/\left|\tilde{L}^*\right| \leq o(1). \tag{8}$$

**Remark 3** *Theorem 2 demonstrates that SGD iterations can converge to weights that achieve a near optimal loss of (1), respectively. This result is of independent interest, as existing training dynamics and convergence analyses for contrastive loss are limited to linear networks. Here, we extend such analysis to nonconvex optimization settings where the network contains nonlinear ReLU activations.*

**Theorem 4 (Unsuccessful learning of ITCP on raw data $S$ with low feature purity in Stage S1)** *For each neuron pair $(\bar{w}_i, \bar{v}_i)$ in $(\overline{\mathbf{W}}, \overline{\mathbf{V}})$, there exists a spurious feature pair $(j, j') \in [d]$ such that*

$$\bar{w}_i = \alpha_{i,j}\mathbf{M}_j + \alpha_{i,j'}\mathbf{M}_{j'} + \mathbf{r}_i, \quad \bar{v}_i = \alpha_{i,j}\mathbf{H}_j + \alpha_{i,j'}\mathbf{H}_{j'} + \mathbf{s}_i \tag{9}$$

*where $\alpha_{i,j}^2, \alpha_{i,j'}^2 = \Theta\left(\|\bar{w}_i\|_2^2 + \|\bar{v}_i\|_2^2\right)$ and $\|\mathbf{r}_i\|_2^2, \|\mathbf{s}_i\|_2^2 \leq O((\|\bar{w}_i\|_2^2 + \|\bar{v}_i\|_2^2)/d)$. Moreover, for every spuriously correlated pair $(j, j')$, there exist at least $\Omega(1)$ neuron pairs $(\bar{w}_i, \bar{v}_i)$ that primarily learn the mixed feature pair $(\mathbf{M}_j, \mathbf{H}_j), (\mathbf{M}_{j'}, \mathbf{H}_{j'})$.*

**Remark 5** *Theorem 4 shows that ITCP on raw data yields low feature purity. Each neuron pair $(\bar{w}_i, \bar{v}_i)$ learns a mixture of features, with $\mathbf{M}_j$ entangled with $\mathbf{M}_{j'}$ and likewise for $\mathbf{H}_j$ and $\mathbf{H}_{j'}$. Thus, the learned weights $\overline{\mathbf{W}}$ and $\overline{\mathbf{V}}$ fail to separate features $j$ and $j'$, degrading downstream performance.*

**Theorem 6 (Spurious feature suppression and relevant feature preservation by recaption)** *After $T = \Theta(d \log d)$ steps of SGD, the decoder $G$ in (6), finetuned by solving (7), converges to weights $(\hat{\mathbf{W}}, \hat{\mathbf{V}})$ with expected loss $L_C \leq \Theta(1/d)$. The recaptioned texts in $\tilde{S}_w$ are computed by $\hat{y}_p = G(x_p)$. Then for any index $j \in [d]$ such that $|z_{x_p}^j| = 1$, the decoder output satisfies:*

$$\Pr(z_{\hat{y}_p}^j = 1 \mid |z_{x_p}^j| = 1) \geq 1 - \Theta\left(1/d\right), \quad \Pr(z_{\hat{y}_p}^{j'} = 1 \mid |z_{x_p}^j| = 1) \leq \Theta\left(1/d\right), \quad \forall j' \neq j. \tag{10}$$

**Remark 7** *After captioning and filtering, the text in $\tilde{S}_w$ contains fewer spurious features and more aligned pairs than in raw data $S_w$. Under Assumption 3, the spurious feature probability drops from $C_s$ to $\Theta(1/d)$, while the chance of retaining all aligned features increases from $C_s$ to $1 - \Theta(1/d)$. The resulting dataset $\tilde{S} = S_h \cup \tilde{S}_w$ thus provides better-aligned pairs for contrastive learning, leading to higher feature purity. We next show how ITCP trained on $\tilde{S}$ improves purity.*

**Theorem 8 (Successful learning of ITCP on filtered data $\tilde{S}$ with high feature purity in Stage S4)** *Each $(\tilde{w}_i, \tilde{v}_i)$ in $(\widetilde{\mathbf{W}}, \widetilde{\mathbf{V}})$ primarily learns some $(\mathbf{M}_j, \mathbf{H}_j)$ with $j \in [d]$:*

$$\tilde{w}_i = \tilde{\alpha}_{i,j}\mathbf{M}_j + \tilde{\mathbf{r}}_i, \quad \tilde{v}_i = \tilde{\alpha}_{i,j}\mathbf{H}_j + \tilde{\mathbf{s}}_i \tag{11}$$

*where $\tilde{\alpha}_{i,j}^2 = \Theta(\|\tilde{w}_i\|_2^2 + \|\tilde{v}_i\|_2^2)$ and $\|\tilde{\mathbf{r}}_i\|_2^2, \|\tilde{\mathbf{s}}_i\|_2^2 \leq O\left((\|\tilde{w}_i\|_2^2 + \|\tilde{v}_i\|_2^2)/d\right)$. For each $j \in [d]$, at least $\Omega(1)$ neuron pairs $(\tilde{w}_i, \tilde{v}_i)$ primarily learn purified feature pair $(\mathbf{M}_j, \mathbf{H}_j)$.*

**Remark 9** *Theorem 8 indicates that the model learned by ITCP on filtered data achieves a purified representation. Specifically, a neuron pair $(\tilde{w}_i, \tilde{v}_i)$ learns one single feature pair $(\mathbf{M}_j, \mathbf{H}_j)$, respectively. As a result, $\widetilde{\mathbf{W}}$ and $\widetilde{\mathbf{V}}$ yield purified representations that effectively separate individual features, enabling improved downstream performance.*

### 4.2. Performance Comparison on Downstream Tasks

We next compare the performance of the models $(f_{\overline{\mathbf{W}}}, g_{\overline{\mathbf{V}}})$ and $(f_{\widetilde{\mathbf{W}}}, g_{\widetilde{\mathbf{V}}})$ on the zero-shot image classification problem with out-of-domain data described in Appendix B.5.

**Theorem 10 (Zero-Shot Image Classification)**

*For the OOD zero-shot $K$-class image classification problem, the model ($f_{\overline{\mathbf{W}}}$, $g_{\overline{\mathbf{V}}}$) from ITCP using raw data has a constant failure probability:*

$$\Pr\left(\arg\max_{k\in[K]}\langle f_{\overline{\mathbf{W}}}(x), g_{\overline{\mathbf{V}}}(y_k)\rangle = l_x\right) = 1 - \Theta(1);. \tag{12}$$

*In contrast, the model ($f_{\widetilde{\mathbf{W}}}$, $g_{\widetilde{\mathbf{V}}}$) from ITCP using filtered caption succeeds with high probability:*

$$\Pr\left(\arg\max_{k\in[K]}\langle f_{\widetilde{\mathbf{W}}}(x), g_{\widetilde{\mathbf{V}}}(y_k)\rangle = l_x\right) = 1 - o(1). \tag{13}$$

**Remark 11** *Theorem 10 first shows that the zero-shot performance of $(f_{\overline{\mathbf{W}}}, g_{\overline{\mathbf{V}}})$ is poor due to low feature purity, as established in Theorem 4. It further shows that $(f_{\widetilde{\mathbf{W}}}, g_{\widetilde{\mathbf{V}}})$ achieves accurate classification, owing to high feature purity from Theorem 8. Notably, this result holds under distribution shift in the test images.*

## References


[1] Zeyuan Allen-Zhu and Yuanzhi Li. Feature purification: How adversarial training performs robust deep learning. In *2021 IEEE 62nd Annual Symposium on Foundations of Computer Science (FOCS)*, pages 977–988. IEEE, 2022.

[2] Chenxin An, Jiangtao Feng, Kai Lv, Lingpeng Kong, Xipeng Qiu, and Xuanjing Huang. Cont: Contrastive neural text generation. *Advances in Neural Information Processing Systems*, 35: 2197–2210, 2022.

[3] Soravit Changpinyo, Piyush Sharma, Nan Ding, and Radu Soricut. Conceptual 12m: Pushing web-scale image-text pre-training to recognize long-tail visual concepts. In *Proceedings of the IEEE/CVF conference on computer vision and pattern recognition*, pages 3558–3568, 2021.

[4] Zixiang Chen, Yihe Deng, Yuanzhi Li, and Quanquan Gu. Understanding transferable representation learning and zero-shot transfer in clip. In *Proceedings of the 12th International Conference on Learning Representations (ICLR)*, Vienna, Austria, 2024.

[5] Karan Desai and Justin Johnson. Redcaps: Web-curated image-text data for robust image captioning. In *NeurIPS*, 2021.

[6] Lijie Fan, Dilip Krishnan, Phillip Isola, Dina Katabi, and Yonglong Tian. Improving clip training with language rewrites. *Advances in Neural Information Processing Systems*, 36: 35544–35575, 2023.

[7] Jeff Z HaoChen, Colin Wei, Adrien Gaidon, and Tengyu Ma. Provable guarantees for self-supervised deep learning with spectral contrastive loss. *Advances in Neural Information Processing Systems*, 34:5000–5011, 2021.

[8] Xiaowei Hu, Zhe Gan, Jianfeng Wang, Zhengyuan Yang, Zicheng Liu, Yumao Lu, and Lijuan Wang. Scaling up vision-language pre-training for image captioning. In *Proceedings of the IEEE/CVF conference on computer vision and pattern recognition*, pages 17980–17989, 2022.

[9] Yu Huang, Chenzhuang Du, Zihui Xue, Xuanyao Chen, Hang Zhao, and Longbo Huang. What makes multi-modal learning better than single (provably). *Advances in Neural Information Processing Systems*, 34:10944–10956, 2021.

[10] Chao Jia, Yinfei Yang, Ye Xia, Yi-Ting Chen, Zarana Parekh, Hieu Pham, Quoc Le, Yun-Hsuan Sung, Zhen Li, and Tom Duerig. Scaling up visual and vision-language representation learning with noisy text supervision. In *International conference on machine learning*, pages 4904–4916. PMLR, 2021.

[11] Jason D Lee, Qi Lei, Nikunj Saunshi, and Jiacheng Zhuo. Predicting what you already know helps: Provable self-supervised learning. *Advances in Neural Information Processing Systems*, 34:309–323, 2021.

[12] Junnan Li, Dongxu Li, Caiming Xiong, and Steven Hoi. Blip: Bootstrapping language-image pre-training for unified vision-language understanding and generation. In *International conference on machine learning*, pages 12888–12900. PMLR, 2022.

[13] Yujie Mo, Zhihe Lu, Runpeng Yu, Xiaofeng Zhu, and Xinchao Wang. Revisiting self-supervised heterogeneous graph learning from spectral clustering perspective. *Advances in Neural Information Processing Systems*, 37:43133–43163, 2024.

[14] Ryumei Nakada, Halil Ibrahim Gulluk, Zhun Deng, Wenlong Ji, James Zou, and Linjun Zhang. Understanding multimodal contrastive learning and incorporating unpaired data. In *International Conference on Artificial Intelligence and Statistics*, pages 4348–4380. PMLR, 2023.

[15] Thao Nguyen, Samir Yitzhak Gadre, Gabriel Ilharco, Sewoong Oh, and Ludwig Schmidt. Improving multimodal datasets with image captioning. *Advances in Neural Information Processing Systems*, 36, 2024.

[16] Alec Radford, Jong Wook Kim, Chris Hallacy, Aditya Ramesh, Gabriel Goh, Sandhini Agarwal, Girish Sastry, Amanda Askell, Pamela Mishkin, Jack Clark, et al. Learning transferable visual models from natural language supervision. In *International conference on machine learning*, pages 8748–8763. PMLR, 2021.

[17] Noam Rotstein, David Bensaïd, Shaked Brody, Roy Ganz, and Ron Kimmel. Fusecap: Leveraging large language models for enriched fused image captions. In *Proceedings of the IEEE/CVF Winter Conference on Applications of Computer Vision*, pages 5689–5700, 2024.

[18] Christoph Schuhmann, Robert Beaumont, Richard Vencu, et al. Laion-400m: Open dataset of clip-filtered 400 million image-text pairs, 2021. arXiv preprint arXiv:2111.02114.

[19] Piyush Sharma, Nan Ding, Sebastian Goodman, and Radu Soricut. Conceptual captions: A cleaned, hypernymed, image alt-text dataset for automatic image captioning. In *Proceedings of ACL*, 2018.

[20] Jianfeng Wang, Zhengyuan Yang, Xiaowei Hu, Linjie Li, Kevin Lin, Zhe Gan, Zicheng Liu, Ce Liu, and Lijuan Wang. Git: A generative image-to-text transformer for vision and language. *arXiv preprint arXiv:2205.14100*, 2022.

[21] Peng Wang, An Yang, Rui Men, Junyang Lin, Shuai Bai, Zhikang Li, Jianxin Ma, Chang Zhou, Jingren Zhou, and Hongxia Yang. Ofa: Unifying architectures, tasks, and modalities through a simple sequence-to-sequence learning framework. In *International conference on machine learning*, pages 23318–23340. PMLR, 2022.

[22] Wenhui Wang, Hangbo Bao, Li Dong, Johan Bjorck, Zhiliang Peng, Qiang Liu, Kriti Aggarwal, Owais Khan Mohammed, Saksham Singhal, Subhojit Som, et al. Image as a foreign language: Beit pretraining for vision and vision-language tasks. In *Proceedings of the IEEE/CVF Conference on Computer Vision and Pattern Recognition*, pages 19175–19186, 2023.

[23] Zirui Wang, Jiahui Yu, Adams Wei Yu, Zihang Dai, Yulia Tsvetkov, and Yuan Cao. Simvlm: Simple visual language model pretraining with weak supervision. *arXiv preprint arXiv:2108.10904*, 2021.

[24] Zixin Wen and Yuanzhi Li. Toward understanding the feature learning process of self-supervised contrastive learning. In *International Conference on Machine Learning*, pages 11112–11122. PMLR, 2021.

[25] Chunlin Yu, Ye Shi, and Jingya Wang. Contextually affinitive neighborhood refinery for deep clustering. *Advances in Neural Information Processing Systems*, 36:5778–5790, 2023.

[26] Jiahui Yu, Zirui Wang, Vijay Vasudevan, Legg Yeung, Mojtaba Seyedhosseini, and Yonghui Wu. Coca: Contrastive captioners are image-text foundation models. *arXiv preprint arXiv:2205.01917*, 2022.

[27] Qi Zhang, Yifei Wang, and Yisen Wang. On the generalization of multi-modal contrastive learning. In *International Conference on Machine Learning*, pages 41677–41693. PMLR, 2023.

[28] Xiang Zhang, Ziyuan Zhao, Theodoros Tsiligkaridis, and Marinka Zitnik. Self-supervised contrastive pre-training for time series via time-frequency consistency. *Advances in neural information processing systems*, 35:3988–4003, 2022.

The overall structure of the appendix is as follows. Each appendix provides supplementary information that supports the main content of this document but is not included in the main body to maintain clarity and flow.

- **Appendix A: Experiments**
  Experiments include both synthetic simulations and CLIP/LaCLIP evaluations on real datasets.
- **Appendix B: Preliminaries**
  Mathematical preliminaries and notation used throughout the paper. A *proof sketch* is also provided to outline the key ideas behind the main results.
- **Appendix C: Technical Lemmas**
  Full statements and proofs of supporting lemmas used in the theoretical analysis.
- **Appendix D–J: Proofs and Theoretical Analysis**
  - **Appendix D–F: ITCP on Raw Data (Phase I–III)**
    Theoretical proof of ITCP across three training phases on raw data.
  - **Appendix G: Captioning**
    Theoretical proof of reception using high quality data.
  - **Appendix H: Filtering**
    Theoretical proof of filtering noisy caption-text pairs.
  - **Appendix I: ITCP on Synthetic (Recaptioned) Data**
    Theoretical proof of training dynamics when using synthetic recaptions.
  - **Appendix J: Downstream Task Evaluation**
    Theoretical implications for performance on downstream tasks.

## Appendix A. Experiment

All experiments were conducted on an internal compute cluster using 8 NVIDIA A5000 GPUs with 24 GB memory each, and each run completed within 50 GPU-hours. No large-scale pretraining or resource-intensive tuning was performed beyond the reported experiments.

### A.1. Simulated Experiment

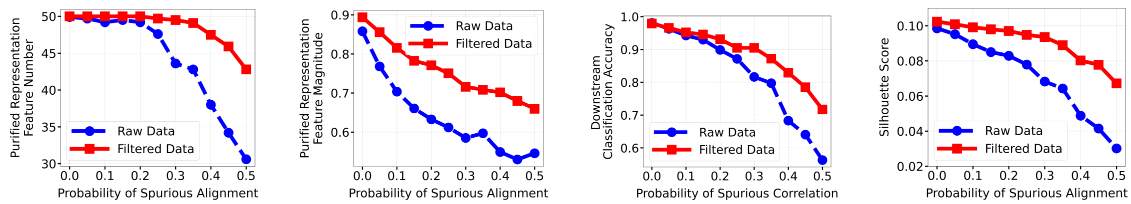


Figure 1: Performance comparison of ITCP on raw data and filtered (recaptioned) data when the probability of spurious correlation $C_s$ changes. (a) Number of features that have purified representation in the model (b) Average magnitude of purified presentations (c) Zero-shot out-of-domain classification accuracy (d) Silhouette Score with cosine distance.

**Experiment Setup.** We first validate our results via simulated experiments, using the same framework from Section 2.1. We adopt a more general spurious correlation model than Assumption 3, allowing each $\mathbf{M}_j$ to be spuriously linked with multiple $\mathbf{H}_{j'}$ ($j' \neq j$), while keeping the total spurious correlation probability at $C_s$. We set $d_1 = 2500$, $d = 50$, $|S_w| = 5000$, $|S_h| = 1000$, and use $m = 80$ neurons. Matrices $\mathbf{M}, \mathbf{H}$ are drawn from standard Gaussians and orthonormalized via QR decomposition. Sparse codes $z_x$ follows Bernoulli$(0.1)$ Noise variance $\sigma_\xi^2 = 1/d$. SGD runs with batch size 500 and step size 0.001. Downstream evaluation uses 5-way classification with test $z_x \sim$ Bernoulli$(0.2)$; class codes $z_{y_k}$ partition the $d$-dim space. Results are averaged over 20 trials. Models $(\overline{\mathbf{W}}, \overline{\mathbf{V}})$ and $(\widetilde{\mathbf{W}}, \widetilde{\mathbf{V}})$ are trained on raw and filtered data, respectively.

**Improved feature representation using filtered (recaptioned) data.** We say a weight $\bar{w}_i$ learn a *purified representation* of $\mathbf{M}_j$ if its projection along $\mathbf{M}_j$ achieves the largest magnitude and satisfies $|\langle \bar{w}_i, \mathbf{M}_j \rangle| / \|\bar{w}_i\| > 0.5$. The same applies to $(\widetilde{\mathbf{W}}, \widetilde{\mathbf{V}})$. Figure 1(a) shows the number of features $\mathbf{M}_j$ (out of $d = 50$ total features) for which at least one neuron in $\overline{\mathbf{W}}$ (or $\widetilde{\mathbf{W}}$, respectively) learns a purified representation. The results show that ITCP trained on filtered data learns purified representations for nearly all features, even at high spurious correlation levels ($C_s = 0.3$). In contrast, ITCP on raw data degrades significantly, with purity dropping faster as $C_s$ increases. Moreover, Figure 1(b) shows the average of the largest projection magnitudes among neurons that learn purified features. The magnitude from $\widetilde{\mathbf{W}}$ (ITCP on filtered data) is consistently higher than that from $\overline{\mathbf{W}}$, indicating stronger purified representations. This aligns with Theorems 4, 8 and Remark 9.

**Improved zero-shot out-of-domain performace using filtered (recaptioned) data.** Figure 1(c) compares the classification accuracy of both models on zero-shot out-of-domain data. The model trained on filtered data consistently outperforms the one trained on raw data, with the performance gap widening as spurious correlations in the raw data increase. We also adopt the widely used Silhouette Score (SS) with cosine distance [13, 25, 28] to evaluate feature embedding quality in different clusters, as shown in Figure 1(d). A higher SS indicates better intra-class alignment and inter-class orthogonality, reflecting more purified representations. These results verify Theorem 10.

**Impact of feature purity.** When $C_s$ reaches 0.35 in Figure 1, even the filtered data fails to maintain full feature purification: the number of neurons learning disentangled representations of all $d = 50$ features drops significantly (Figure 1(a)), and the SS (Figure 1(d)) and classification accuracy (Figure 1(c)) both decline sharply. This highlights that *feature purity*—the extent to which each neuron aligns to a single semantic direction—is a key bottleneck in contrastive pretraining and downstream generalization.

**Neurons trained on filtered data exhibit a more concentrated distribution.** Figure 2 visualizes the histograms of $|\langle \bar{v}_i, \mathbf{H}_j\rangle|/\|\bar{v}_i\|$ and $|\langle \tilde{v}_i, \mathbf{H}_j\rangle|/\|\tilde{v}_i\|$ for all $i \in [m]$ and $j \in [d]$. The values of $|\langle \tilde{v}_i, \mathbf{H}_j\rangle|/\|\tilde{v}_i\|$ are more concentrated, typically around 0.05 and 0.7. In contrast, the values for $|\langle \bar{v}_i, \mathbf{H}_j\rangle|/\|\bar{v}_i\|$ are less concentrated. This phenomenon is consistent with Theorem 8, which indicates that for every $\mathbf{H}_j$, certain neurons $\tilde{v}_i$ in $\widetilde{\mathbf{V}}$ predominately learns $\mathbf{H}_j$. In such cases, $|\langle \tilde{v}_i, \mathbf{H}_j\rangle|$ approaches 1, while $|\langle \tilde{v}_i, \mathbf{H}_{j'}\rangle|/\|\tilde{v}_i\|$ approaches 0 for $j' \neq j$. The concentrated values of 0.05 and 0.7 observed in Figure 2 are due to noise in the data. In contrast, feature alignment is less significant for $\overline{\mathbf{V}}$, leading to less concentration of the corresponding values. Similar results are obtained for image encoder $|\langle w_i, \mathbf{M}_j\rangle|$, deferred to Figure 3.

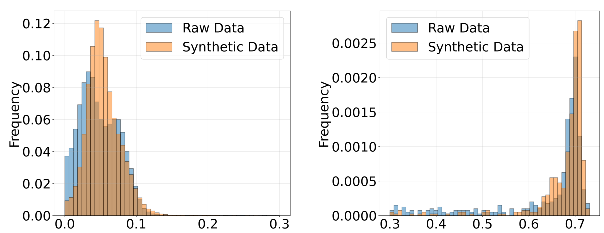


Figure 2: Histogram of $|\langle \bar{v}_i, \mathbf{H}_j\rangle|/\|\bar{v}_i\|$ for ITCP on raw data and $|\langle \tilde{v}_i, \mathbf{H}_j\rangle|/\|\tilde{v}_i\|$ for ITCP on filtered data (split into two figures to highlight the significant differences in the value distributions).

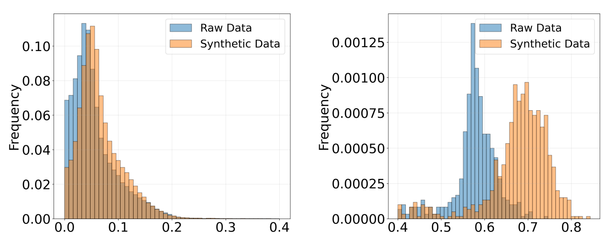


Figure 3: Histogram of $|\langle \bar{w}_i, \mathbf{M}_j\rangle|/|\bar{w}_i|$ for ITCP on raw data and $|\langle \tilde{w}_i, \mathbf{M}_j\rangle|/\tilde{w}_i$ for ITCP on filtered data (split into two figures to highlight the significant differences in the value distributions).

**Enhanced class separation of downstream tasks by ITCP with recaptioned data**. Figure 4 visualizes the t-distributed stochastic neighbor embedding (t-SNE) of the feature embeddings generated by the two models, computed as $f_{\overline{\mathbf{W}}}(x_p)$ and $f_{\widetilde{\mathbf{W}}}(x_p)$ for each $x_p$, respectively. The t-SNE

Table 1: Comparison of CLIP and LaCLIP on Accuracy (%) and Silhouette Score.

| Model | Food-101 Acc | Food-101 SS | CIFAR-10 Acc | CIFAR-10 SS | Caltech-101 Acc | Caltech-101 SS | CIFAR-100 Acc | CIFAR-100 SS | Pets Acc | Pets SS | STL-10 Acc | STL-10 SS |
|---|---|---|---|---|---|---|---|---|---|---|---|---|
| CC12M CLIP | 50.8 | 0.034 | 64.9 | 0.113 | 77.4 | 0.225 | 38.5 | 0.005 | 64.1 | 0.069 | 91.0 | 0.195 |
| CC12M LaCLIP | **60.7** | **0.038** | **75.1** | **0.157** | **83.3** | **0.276** | **43.9** | **0.029** | **72.4** | **0.070** | **95.1** | **0.273** |
| RedCaps CLIP | 81.5 | 0.125 | 70.4 | 0.100 | 72.8 | 0.210 | 39.9 | −0.002 | **82.7** | **0.091** | **92.8** | 0.226 |
| RedCaps LaCLIP | **85.0** | **0.175** | **74.8** | **0.107** | **76.4** | **0.233** | **40.7** | **0.011** | 78.2 | 0.074 | 91.4 | **0.275** |
| LAION CLIP | 85.5 | 0.116 | 93.0 | 0.181 | 91.2 | 0.258 | 71.7 | 0.078 | 90.1 | 0.122 | 97.3 | 0.223 |
| LAION LaCLIP | **86.5** | **0.148** | **93.5** | **0.215** | **92.4** | **0.306** | **73.9** | **0.108** | **90.9** | **0.152** | **98.4** | **0.260** |

method projects the high-dimensional embeddings onto a two-dimensional map. One can see that the embeddings from different groups are more distinctly separated in the model trained using ITCP on recaptioned data, indicating that this approach achieves better feature alignment.

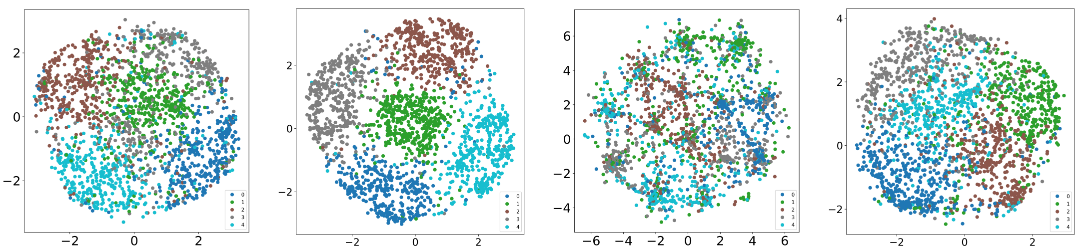

(*a*) Raw ($C_s = 0.3$) (*b*) Recaption ($C_s = 0.3$) (*c*) Raw ($C_s = 0.5$) (*d*) Recaption ($C_s = 0.5$)

Figure 4: t-SNE visualization of text embedding with spurious correlation probability $C_s$.

## A.2. Experiments on Practical Data and Models

**LaCLIP improves generalization over CLIP via recaption.** Tables 1 compare CLIP [16] and LaCLIP [6], which share the same architecture and datasets, except LaCLIP replaces part of the original captions with LLM-generated rewrites. "CC12M CLIP" denotes a CLIP model pretrained on raw CC12M [3], while "CC12M LaCLIP" uses the same model and data but with LLM-rewritten captions. Other models are obtained similarly using RedCaps [5] and LAION [18] datasets. We evaluate their zero-shot classification accuracy and Silhouette Scores on various downstream datasets. LaCLIP generally outperforms CLIP in both metrics, empirically validating that higher-quality captions improve zero-shot generalization.

Next, we study the feature purity using a CLIP model pretrained on CC3M [19]. Both the image and text encoders are 12-layer transformers that produce features in $\mathbb{R}^{768}$, which are subsequently projected into a shared embedding space of $\mathbb{R}^{512}$ through final linear projection layers, as illustrated in Figure 6. The final linear projection layer has 512 neurons and is functionally aligned with $\mathbf{V}$ in our theoretical model. We now present two key findings from this setting:

**Purified neurons enhance generalization.** To investigate the effect of feature purity on generalization, we prune the neurons in the final linear layer in different ways and evaluate the resulting zero-shot classification performance. Specifically, we rank the 512 neurons by their average pairwise absolute cosine similarity to all other neurons, from lowest to highest. The absolute cosine similarity of neurons $v_j$, $v_{j'}$ is computed as $|\langle v_j, v_{j'} \rangle| / \|v_j\| \|v_{j'}\|$ for all $j, j' \in \{1, 2, \ldots, 512\}$. A lower average indicates higher feature purity (i.e., more orthogonal representations), while a higher value suggests feature mixing. We evaluate three pruning strategies: (1) retaining **high-purity** neurons, i.e., with lowest similarity, (2) retaining **low-purity** neurons, i.e., with highest similarity, and (3) retaining a **random** subset of neurons. The number of retained neurons is varied from 200 to 500. As shown in Figure 5 (a-c,e-g), downstream performance is the best when retaining high-purity neurons, followed by random selection, with low-purity neurons performing the worst. These results highlight the critical role of purified features in downstream generalization.

**Data misalignment reduces feature purity.** To study how image-text misalignment affects feature purity, we randomly shuffling texts across image-text pairs in CC3M with probability $C_m$, as illustrated in Figure 7, thereby introducing a controlled probability of modality misalignment. We then use the shuffled dataset to fine-tune the last linear projection layer only of the pretrained CLIP model, freezing other layers. We then compute the cosine similarities of all 512 neuron weight vectors $v_j \in \mathbb{R}^{768}$ of the fine-tuned model. Figure 5 (d) reports the average absolute cosine similarity of all neuron pairs, while (h) presents a histogram of cosine similarity $\langle v_j, v_{j'} \rangle / (\|v_j\| \|v_{j'}\|)$. One can see that as $C_m$ increases, the average absolute cosine similarity increases, and the neurons become less orthogonal to each other and tend to encode mixed representations, resulting in lower feature purity. This coincides with the decreases classification accuracy in downstream tasks, as shown in Table 2.

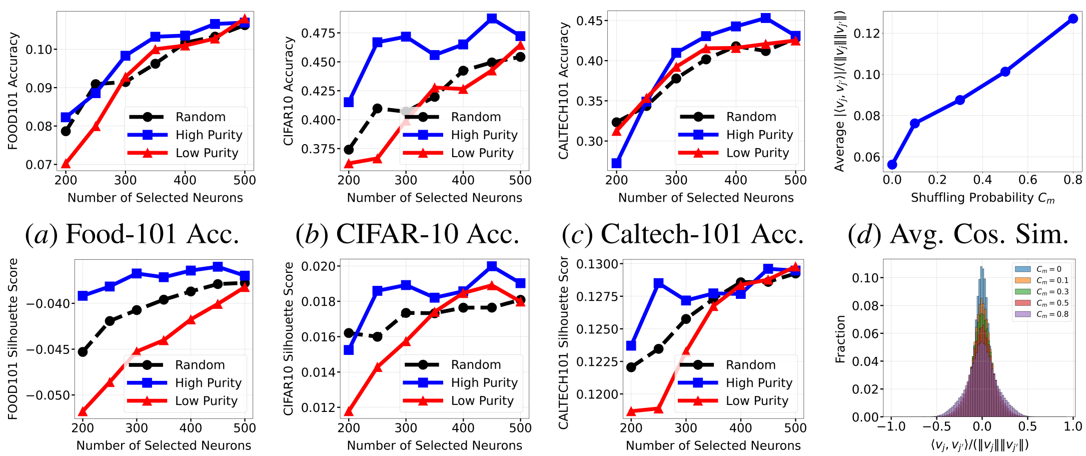


($a$) Food-101 Acc. ($b$) CIFAR-10 Acc. ($c$) Caltech-101 Acc. ($d$) Avg. Cos. Sim.

($e$) Food-101 SS ($f$) CIFAR-10 SS ($g$) Caltech-101 SS ($h$) Hist of Cos. Sim.

Figure 5: Left (a–c,e-g): Retaining high-purity neurons outperform random and low-purity neurons in downstream tasks. More datasets shown in Figure 8. Right(d,h): When $C_m$ increases, the neurons have higher cosine similarity and reduced feature purity.

**CLIP architecture.** Figure 6 illustrates the CLIP architecture used in our experiments. Both image and text inputs are independently encoded by 12-layer transformer backbones, each producing a 768-dimensional feature vector. These features are then projected into a shared 512-dimensional embedding space through learned linear projection matrices $\mathbf{W} \in \mathbb{R}^{768\times512}$ and $\mathbf{V} \in \mathbb{R}^{768\times512}$, corresponding to the image and text encoders in our theorem, defined in Eq. (2). The resulting embeddings are aligned via a contrastive loss that maximizes similarity for matched image-text pairs while minimizing similarity for unmatched pairs. This architecture forms the foundation for our analyses on neuron selection and feature purity in the shared embedding space.

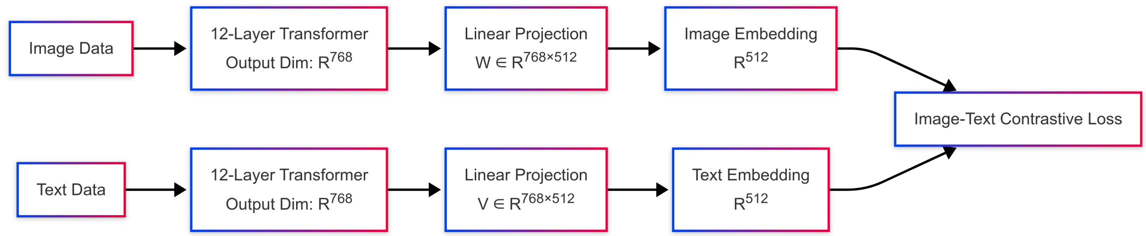


Figure 6: Architecture of CLIP used in our experiments. Both image and text encoders are 12-layer transformers that output features in $\mathbb{R}^{768}$, which are then projected into a shared $\mathbb{R}^{512}$ embedding space via final linear projection layers $\mathbf{W}$ and $\mathbf{V}$, corresponding to Eq. (2) and Eq. (3) in our theoretical analysis. Contrastive loss is computed between the resulting image and text embeddings.

**Simulating Modality Misalignment via Caption Shuffling.** Figure 7 illustrates how modality misalignment is introduced by randomly shuffling text captions across image-text pairs with probability $C_m$, resulting in noisy supervision for contrastive learning.

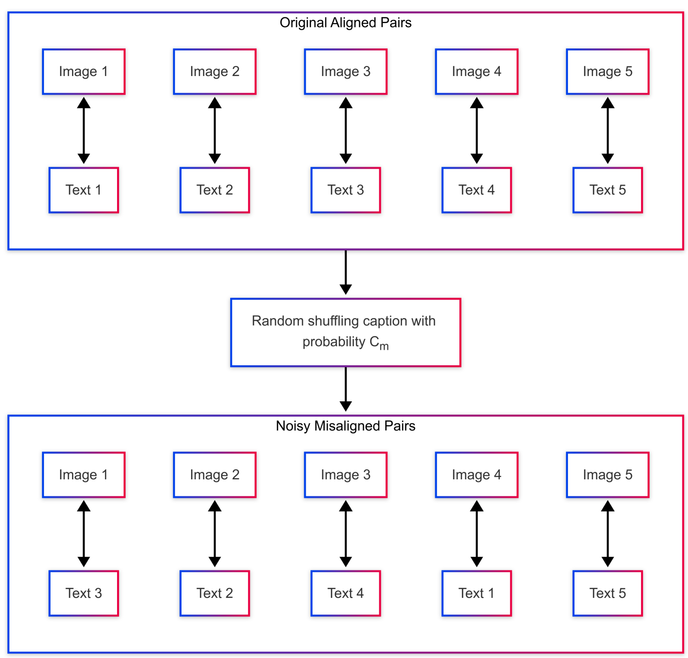


Figure 7: Simulating Modality Misalignment via Caption Shuffling. Starting from original aligned image-text pairs, a controlled probability $C_m$ of misalignment is introduced by randomly shuffling the text captions. This results in noisy pairs that reflect varying levels of spurious correlations.

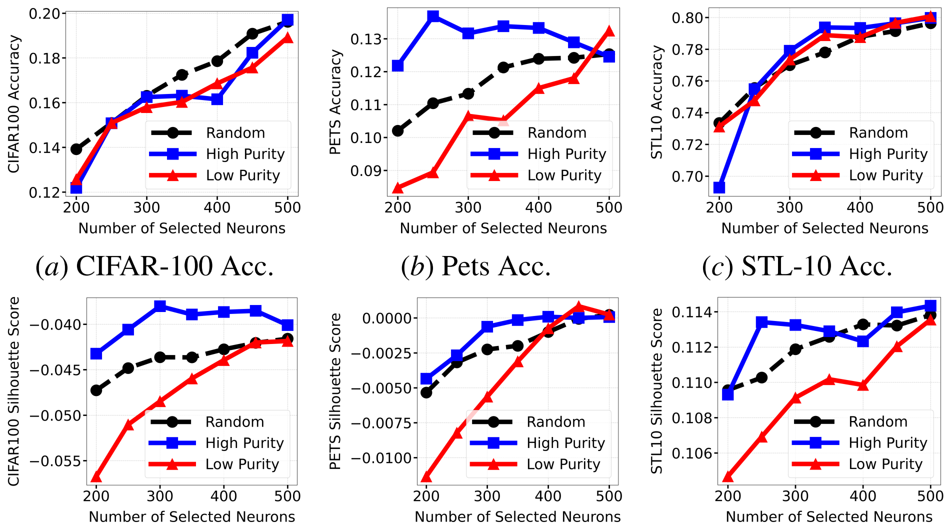


(a) CIFAR-100 Acc. (b) Pets Acc. (c) STL-10 Acc.

(d) CIFAR-100 SS (e) Pets SS (f) STL-10 SS

Figure 8: Zero-shot classification accuracy (top) and Silhouette Score (bottom) under different neuron selection strategies for CIFAR-100, Pets, and STL-10 datasets.

Table 2: Accuracy (%) and Silhouette Score of CLIP models finetuned with varying $C_m$ on six datasets.

| **Dataset** | $C_m = 0$ | | $C_m = 0.1$ | | $C_m = 0.3$ | | $C_m = 0.5$ | | $C_m = 0.8$ | |
|---|---|---|---|---|---|---|---|---|---|---|
| | Acc | SS | Acc | SS | Acc | SS | Acc | SS | Acc | SS |
| Caltech101 | 59.7 | 0.160 | 48.2 | 0.124 | 47.9 | 0.121 | 43.6 | 0.117 | 44.5 | 0.115 |
| CIFAR-10 | 57.9 | 0.030 | 50.7 | 0.012 | 49.5 | 0.013 | 46.5 | 0.013 | 44.1 | 0.011 |
| CIFAR-100 | 26.4 | −0.038 | 19.5 | −0.042 | 17.8 | −0.043 | 17.4 | −0.044 | 16.2 | −0.048 |
| Food-101 | 12.9 | −0.073 | 10.9 | −0.052 | 10.9 | −0.056 | 11.1 | −0.057 | 11.1 | −0.059 |
| Pets | 13.9 | −0.005 | 13.3 | −0.006 | 13.2 | −0.009 | 13.4 | −0.011 | 12.6 | −0.012 |
| STL-10 | 86.3 | 0.164 | 79.8 | 0.103 | 79.2 | 0.102 | 78.8 | 0.100 | 78.3 | 0.097 |

**Purified neuron selection enhances generalization.** Figure 8 presents additional experimental results on CIFAR-100, Pets, and STL-10, complementing the main results reported in Figure 5. Due to space constraints, we include only Food-101, CIFAR-10, and Caltech-101 in the main text. All experiments follow the same protocol, evaluating zero-shot classification accuracy and Silhouette Score under different neuron selection strategies. These results consistently support our core finding: selecting high-purity neurons leads to improved downstream performance across diverse datasets.

**Higher shuffling probability leads to reduced generalization and feature purity.** Table 2 presents additional experimental results on CLIP models finetuned with different levels of randomly shuffling probability $C_m$ to simulate spurious correlation, showing that both accuracy and Silhouette Score consistently decrease as $C_m$ increases.

## Appendix B. Preliminaries

We first restate some important notations used in the Appendix, which are summarized in Table 3.

Table 3: Summary of Notations

| Notations | Annotation |
|---|---|
| $\mathbf{M} \in \mathbb{R}^{d_1 \times d}$, $\mathbf{H} \in \mathbb{R}^{d_1 \times d}$ | $\mathbf{M}$ is the image dictionary matrix, $\mathbf{H}$ is the text dictionary matrix. |
| $\mathbf{W} \in \mathbb{R}^{m \times d_1}$, $\mathbf{V} \in \mathbb{R}^{m \times d_1}$ | $\mathbf{W}$ is the weight of image encoder, $\mathbf{V}$ is the weight of text encoder. |
| $x_p \in \mathbb{R}^{d_1}, y_p \in \mathbb{R}^{d_1}$ | $x_p$ and $y_p$ represent an image and a text data, respectively. |
| $z_{x_p}, z_{y_p} \in \mathbb{R}^d$ | $z_{x_p}$ and $z_{y_p}$ are the sparse signals of image and text, respectively. $z_{y_k}$ is the sparse signal for the text prompt $y_k$. |
| $z^j_{x_p}, z^j_{y_p}$ | $z^j_{x_p}$ is the $j$-th coordinate of $z_{x_p}$; $z^j_{y_p}$ is the $j$-th coordinate of $z_{y_p}$. |
| $L$, $L_C$ | $L$ is the loss for ITCP; $L_C$ is the loss for Image-grounded Text Decoding. |
| $S = S_h \cup S_w$ | $S_w$ is the noisy web low-quality dataset; $S_h$ is the human-annotated high-quality dataset. |
| $\tilde{S} = S_h \cup \tilde{S}_w$ | $\tilde{S}_w$ replaces noisy captions in $S_w$ with synthetic captions. |
| $T_1$ | Phase I of ITCP with $b_i^{(t)} = 0$. |
| $T_2$ | Phase II of ITCP with $b_i^{(t+1)} = (1 + \frac{\eta}{d})b_i^{(t)}$. |
| $T_3$ | Phase III of ITCP with $b_i^{(t+1)} = b_i^{(T_2)}$. |
| $T_C$ | Stage of training caption generators. |
| $\mathcal{S}_{j,\text{sure}}$ | The set of well-initialized neurons $(w_i, v_i)$ on features $(\mathbf{M}_j, \mathbf{H}_j)$. |

### B.1. Proof Scratch

Theorem 2 is proven by integrating the convergence analyses in Appendix F and Appendix I. Appendix F establishes convergence for ITCP on raw data, while Appendix I extends the convergence result to ITCP on synthetic data. Together, they verify that SGD with ReLU networks achieves near-optimal contrastive loss on both datasets.

Theorem 4 is proven across Appendix D, Appendix E, and Appendix F. Specifically, Appendix D models Phase I training ($t \leq T_1$) and proves that neurons simultaneously align with true features and spuriously correlated features due to comparable gradient contributions, preventing pure feature separation. Appendix E analyzes Phase II training ($T_1 < t \leq T_2$) and shows that this spurious alignment continues to strengthen, as neurons with initial mixed alignment further amplify their entanglement during continued SGD updates. Appendix F establishes the convergence behavior during Phase III ($T_2 < t \leq T_3$), showing that the network stabilizes into mixed solutions where each neuron represents a combination of multiple features. These detailed stages collectively prove the failure of purified feature alignment as formalized in Theorem 4.

Theorem 6 is proven across Appendix G and Appendix H. Specifically, Appendix G analyzes the captioning stage, where the decoder is fine-tuned on clean data to generate synthetic captions. It proves that for neurons aligned with true features, the alignment towards the true features grows exponentially while the alignment towards spurious features remains negligible. This ensures that the synthetic captions preserve relevant features and suppress spurious ones. Appendix H then formalizes the filtering process, demonstrating that after replacing noisy captions with synthetic ones, the resulting dataset satisfies much stronger feature purity conditions, with spurious correlations suppressed to $\Theta(1/d)$ and true features preserved with probability $1 - \Theta(1/d)$. These results directly support the purified feature learning described in Theorem 6.

Theorem 8 is proven in Appendix I, which integrates the proofs of Phase I, Phase II, and Phase III for ITCP on synthetic data. Specifically, Appendix I first establishes in Phase I that purified training pairs allow neurons aligned with true features to grow exponentially without spurious interference. It then shows in Phase II that these alignments continue to strengthen while suppressing non-informative neurons, leading to clear feature separation. Finally, it proves in Phase III that the model converges, achieving a bounded final loss and dominant true feature alignment. Since the overall proof structure closely mirrors that of Theorem 4 (which was proven separately across Appendix D, Appendix E, and Appendix F), we consolidate all stages into a single appendix for brevity and clarity.

Theorem 10 is proven in Appendix J, which analyzes the downstream zero-shot classification. Appendix J shows that for ITCP on raw data, spurious features cause a constant classification error, while for ITCP on synthetic data, true and spurious features become separable with high probability, leading to an $o(1)$ error rate. This directly supports the main text conclusion on downstream generalization.

### B.2. Feature Coupling and Expected Values in $S_w$

The following Assumption 4 corresponds to the more specific forms of Assumptions 2 and 3 discussed earlier.

**Assumption 4 (High and low quality pairs)** *The high-quality image-text pairs in $S_h$ have size $|S_h| = \Theta(d^2)$. The low-quality image-text pairs in $S_w$ have size $|S_w| = poly(d)| \gg \omega(d^2)$.*

*In $S_h$, for a positive pair $(x_p, y_p)$, we assume perfect alignment, meaning $z_{x_p} = z_{y_p}$. Consequently, the following holds:*

$$\mathbb{E}\left[z_{x_p}^j z_{y_p}^j\right] = \frac{C_z}{d}, \quad \mathbb{E}\left[z_{x_p}^j z_{y_p}^{j'}\right] = \Theta\left(\frac{1}{d^2}\right), \quad j' \neq j \tag{14}$$

*To model the misaligned features in low-quality pairs in $S_w$, where spurious misalignment occurs at a non-negligible level, we assume $[d]$ can be divided into $d/2$ disjoint sets, each containing exactly two entries. Let $(j, j') \subset [d]$ denote one such set, referred to as a "spuriously correlated set." The following assumptions capture the nature of spurious and true alignments:*

$$\begin{aligned} &\Pr(|z_{y_p}^{j'}| = 1 \mid |z_{x_p}^j| = 1) = \Theta(1) < \frac{1}{2}, \\ &\Pr(|z_{y_p}^{j'}| = 1 \mid |z_{x_p}^j| = 1) + \Pr(|z_{y_p}^{j}| = 1 \mid |z_{x_p}^j| = 1) = 1. \end{aligned} \tag{15}$$

These assumptions imply that true alignment dominates, with $\Pr(|z_{y_p}^j| = 1 \mid |z_{x_p}^j| = 1) > \frac{1}{2}$, while spurious alignment exists at a constant percentage level, making it non-negligible. The intuition behind this assumption is that each feature $j$ is paired with exactly one spuriously correlated feature $j'$, ensuring that $j$ is not associated with any other feature $j'' \neq j'$. This design simplifies the analysis while effectively capturing the key challenges posed by low-quality data.

Then, for a positive pair $(x_p, y_p)$ with $p$ in $S_w$, we have:

$$\begin{aligned} \mathbb{E}\left[z_{x_p}^j z_{y_p}^j\right] + \mathbb{E}\left[z_{x_p}^j z_{y_p}^{j'}\right] &= \frac{C_z}{d}, \\ \mathbb{E}\left[z_{x_p}^j z_{y_p}^{j'}\right] &= \Theta\left(\frac{1}{d}\right) < \frac{C_z}{2d}. \end{aligned} \tag{16}$$

where $(j, j')$ is a spuriously correlated set.

For negative pairs $(x_p, y_q)$, where $p \neq q$, and $p, q \in S$, we have:

$$\mathbb{E}\left[z_{x_p}^j z_{y_q}^{j'}\right] = \Theta\left(\frac{1}{d^2}\right), \quad \forall j, j' \in [d]. \tag{17}$$

In $S_w$, mismatched text and image pairs are prevalent compared to $S_h$. For a postive pair $(x_p, y_p)$, we assume $\frac{\log(1/c_0)}{2\log d} < \Pr(|z_{y_p}^{j'}| = 1 \mid |z_{x_p}^j| = 1) < \frac{1}{2}$. To model this, we assume that for each primary feature $j \in [d]$, there exists exactly one spurious feature $j'$ such that $j$ and $j'$ are uniquely coupled. This implies that $j$ cannot be associated with any other feature $j'' \neq j'$. Mathematically, the coupling is defined as:

$$\Pr(|z_{y_p}^{j'}| = 1 \mid |z_{x_p}^j| = 1) + \Pr(|z_{y_p}^j| = 1 \mid |z_{x_p}^j| = 1) = 1. \tag{18}$$

For a positive pair $(x_p, y_p)$ in $S_w$, the probabilities of spurious and aligned features are further constrained:

$$\frac{\log(1/c_0)}{2\log d} < \Pr(|z_{y_p}^{j'}| = 1 \mid |z_{x_p}^j| = 1) < \frac{1}{2}, \tag{19}$$

The lower bound is established in Lemma 20.

and:

$$\Pr(|z_{y_p}^j| = 1 \mid |z_{x_p}^j| = 1) = 1 - \Pr(|z_{y_p}^{j'}| = 1 \mid |z_{x_p}^j| = 1). \tag{20}$$

Under these assumptions, the expected values for the aligned and spurious features are calculated as follows:

For the aligned feature $j$, we have:

$$\begin{aligned} \mathbb{E}\left[z_{x_p}^j z_{y_p}^j\right] &= \Pr(|z_{y_p}^j| = 1, |z_{x_p}^j| = 1) \\ &= \Pr(|z_{y_p}^j| = 1 \mid |z_{x_p}^j| = 1) \cdot \Pr(|z_{x_p}^j| = 1) \\ &= \Pr(|z_{y_p}^j| = 1 \mid |z_{x_p}^j| = 1) \cdot \frac{C_z}{d}. \end{aligned} \tag{21}$$

For the spurious feature $j'$, we have:

$$\begin{aligned} \mathbb{E}\left[z_{x_p}^j z_{y_p}^{j'}\right] &= \Pr(|z_{y_p}^{j'}| = 1, |z_{x_p}^j| = 1) \\ &= \Pr(|z_{y_p}^{j'}| = 1 \mid |z_{x_p}^j| = 1) \cdot \Pr(|z_{x_p}^j| = 1) \\ &= \Pr(|z_{y_p}^{j'}| = 1 \mid |z_{x_p}^j| = 1) \cdot \frac{C_z}{d} \end{aligned} \tag{22}$$

The total expected value across both aligned and spurious features satisfies:

$$\mathbb{E}\left[z_{x_p}^j z_{y_p}^j\right] + \mathbb{E}\left[z_{x_p}^j z_{y_p}^{j'}\right] = \frac{C_z}{d} \tag{23}$$

Here, $j'$ denotes the spurious feature associated with $j$.

### B.3. Gradient

The contrastive loss in vision-language models (VLM) is defined as follows:

$$\begin{aligned} L(f^{(t)}, h^{(t)}) = \sum_{p \in S} \Big[ &- \langle f^{(t)}(x_p), h^{(t)}(y_p) \rangle + \sum_{x_n \in \mathfrak{N}'} \frac{\big(\langle f^{(t)}(x_n), h^{(t)}(y_p) \rangle\big)^2}{2\tau} \\ &+ \sum_{y_n \in \mathfrak{N}'} \frac{\big(\langle f^{(t)}(x_p), h^{(t)}(y_n) \rangle\big)^2}{2\tau} \Big], \end{aligned} \tag{24}$$

where $\tau > 0$ is a temperature parameter.

We perform stochastic gradient descent (SGD) on this contrastive loss. Let $f^{(t)}$ and $h^{(t)}$ be the image encoder and text encoder networks at iteration $t$, respectively. The network parameters are updated as follows:

$$w_i^{(t+1)} \leftarrow w_i^{(t)} - \eta \nabla_{w_i} L(f^{(t)}, h^{(t)}), \tag{25}$$

$$v_i^{(t+1)} \leftarrow v_i^{(t)} - \eta \nabla_{v_i} L(f^{(t)}, h^{(t)}), \tag{26}$$

where $b_i^{(t)}$, the bias term, is manually tuned during training and thus excluded from gradient updates.

The gradient of $L(f^{(t)}, h^{(t)})$ with respect to $w_i^{(t)}$ at iteration $t$ is given by:

$$\begin{aligned} \nabla_{w_i} L(f^{(t)}, h^{(t)}) = &- \langle v_i^{(t)}, y_p \rangle x_p \cdot \mathbf{1}_{\left|\langle w_i^{(t)}, x_p \rangle\right| \geq b_i^{(t)}} \cdot \mathbf{1}_{\left|\langle v_i^{(t)}, y_p \rangle\right| \geq b_i^{(t)}} \\ &+ \sum_{x_n \in \mathfrak{N}} \frac{\langle f^{(t)}(x_n), h^{(t)}(y_p) \rangle \langle v_i^{(t)}, y_p \rangle x_n}{\tau} \cdot \mathbf{1}_{\left|\langle w_i^{(t)}, x_n \rangle\right| \geq b_i^{(t)}} \cdot \mathbf{1}_{\left|\langle v_i^{(t)}, y_p \rangle\right| \geq b_i^{(t)}} \\ &+ \sum_{y_n \in \mathfrak{N}} \frac{\langle f^{(t)}(x_p), h^{(t)}(y_n) \rangle \langle v_i^{(t)}, y_n \rangle x_p}{\tau} \cdot \mathbf{1}_{\left|\langle w_i^{(t)}, x_p \rangle\right| \geq b_i^{(t)}} \cdot \mathbf{1}_{\left|\langle v_i^{(t)}, y_n \rangle\right| \geq b_i^{(t)}}. \end{aligned} \tag{27}$$

Similarly, the empirical gradient of $L(f^{(t)}, h^{(t)})$ with respect to $v_i^{(t)}$ is:

$$\begin{aligned} \nabla_{v_i} L(f^{(t)}, h^{(t)}) = &- \langle w_i^{(t)}, x_p \rangle y_p \cdot \mathbf{1}_{\left|\langle w_i^{(t)}, x_p \rangle\right| \geq b_i^{(t)}} \cdot \mathbf{1}_{\left|\langle v_i^{(t)}, y_p \rangle\right| \geq b_i^{(t)}} \\ &+ \sum_{x_n \in \mathfrak{N}} \frac{\langle f^{(t)}(x_n), h^{(t)}(y_p) \rangle \langle w_i^{(t)}, x_n \rangle y_p}{\tau} \cdot \mathbf{1}_{\left|\langle w_i^{(t)}, x_n \rangle\right| \geq b_i^{(t)}} \cdot \mathbf{1}_{\left|\langle v_i^{(t)}, y_p \rangle\right| \geq b_i^{(t)}} \\ &+ \sum_{y_n \in \mathfrak{N}} \frac{\langle f^{(t)}(x_p), h^{(t)}(y_n) \rangle \langle w_i^{(t)}, x_p \rangle y_n}{\tau} \cdot \mathbf{1}_{\left|\langle w_i^{(t)}, x_p \rangle\right| \geq b_i^{(t)}} \cdot \mathbf{1}_{\left|\langle v_i^{(t)}, y_n \rangle\right| \geq b_i^{(t)}}. \end{aligned} \tag{28}$$

### B.4. Alignment Updates

We analyze how each neuron $i \in [m]$ aligns with the feature $\mathbf{M}_j$ during each iteration of SGD. The alignment can be described by the following update rule:

$$\begin{aligned} \langle w_i^{(t+1)}, \mathbf{M}_j \rangle &= \langle w_i^{(t)}, \mathbf{M}_j \rangle - \langle \nabla_{w_i} L(f^{(t)}, h^{(t)}), \mathbf{M}_j \rangle \\ &= \langle w_i^{(t)}, \mathbf{M}_j \rangle + \eta z_x^j z_y^j \langle v_i^{(t)}, \mathbf{H}_j \rangle + \eta z_x^j z_y^{j'} \langle v_i^{(t)}, \mathbf{H}_{j'} \rangle \pm Err_t. \end{aligned} \tag{29}$$

Similarly, for $\langle v_i^{(t+1)}, \mathbf{H}_j \rangle$, the update rule becomes:

$$\begin{aligned} \langle v_i^{(t+1)}, \mathbf{H}_j \rangle &= \langle v_i^{(t)}, \mathbf{H}_j \rangle - \langle \nabla_{v_i} L(f^{(t)}, h^{(t)}), \mathbf{H}_j \rangle \\ &= \langle v_i^{(t)}, \mathbf{H}_j \rangle + \eta z_x^j z_y^j \langle w_i^{(t)}, \mathbf{M}_j \rangle + \eta z_x^j z_y^{j'} \langle w_i^{(t)}, \mathbf{M}_{j'} \rangle \pm Err_t. \end{aligned} \tag{30}$$

Using Lemma 18, we know that with high probability, $\sum_{x_n \in \mathfrak{N}} \frac{\langle f^{(t)}(x_n), h^{(t)}(y_p) \rangle}{\tau} \leq O(\frac{1}{d})$, so in Eq (27) the sum of second term and third term is always less than the first term, until $\langle f^{(t)}(x_n), h^{(t)}(y_p) \rangle = \Theta(d)$.

The updates for the components $\langle w_i^{(t+1)}, \mathbf{M}_j \rangle$, $\langle v_i^{(t+1)}, \mathbf{H}_j \rangle$, $\langle w_i^{(t+1)}, \mathbf{M}_{j'} \rangle$, and $\langle v_i^{(t+1)}, \mathbf{H}_{j'} \rangle$ (where $j'$ represents the spurious aligned feature corresponding to $j$) can be expressed concisely in matrix form as follows:

$$\begin{bmatrix} \langle w_i^{(t+1)}, \mathbf{M}_j \rangle \\ \langle v_i^{(t+1)}, \mathbf{H}_j \rangle \\ \langle w_i^{(t+1)}, \mathbf{M}_{j'} \rangle \\ \langle v_i^{(t+1)}, \mathbf{H}_{j'} \rangle \end{bmatrix} = \begin{bmatrix} a & b & 0 & c \\ b & a & c & 0 \\ 0 & c & a & b \\ c & 0 & b & a \end{bmatrix} \begin{bmatrix} \langle w_i^{(t)}, \mathbf{M}_j \rangle \\ \langle v_i^{(t)}, \mathbf{H}_j \rangle \\ \langle w_i^{(t)}, \mathbf{M}_{j'} \rangle \\ \langle v_i^{(t)}, \mathbf{H}_{j'} \rangle \end{bmatrix} \pm Err_t, \tag{31}$$

where the coefficients are defined as:

$$a = 1, \quad b = z_x^j z_y^j \cdot \mathbf{1}_{\left|\langle w_i^{(t)}, x_p \rangle\right| \geq b_i^{(t)}} \cdot \mathbf{1}_{\left|\langle v_i^{(t)}, y_p \rangle\right| \geq b_i^{(t)}},$$

$$c = z_x^j z_y^{j'} \cdot \mathbf{1}_{\left|\langle w_i^{(t)}, x_p \rangle\right| \geq b_i^{(t)}} \cdot \mathbf{1}_{\left|\langle v_i^{(t)}, y_p \rangle\right| \geq b_i^{(t)}}.$$

Therefore, we have

$$\begin{aligned} \langle w_i^{(t)}, \mathbf{M}_j \rangle = \langle v_i^{(t)}, \mathbf{H}_j \rangle = &\frac{(a+b+c)^t + (a+b-c)^t}{4} \left( \langle w_i^{(0)}, \mathbf{M}_j \rangle + \langle v_i^{(0)}, \mathbf{H}_j \rangle \right) \\ &+ \frac{(a+b+c)^t - (a+b-c)^t}{4} \left( \langle w_i^{(0)}, \mathbf{M}_{j'} \rangle + \langle v_i^{(0)}, \mathbf{H}_{j'} \rangle \right) \end{aligned} \tag{32}$$

and

$$\begin{aligned} \langle w_i^{(t)}, \mathbf{M}_{j'} \rangle = \langle v_i^{(t)}, \mathbf{H}_{j'} \rangle = &\frac{(a+b+c)^t + (a+b-c)^t}{4} \left( \langle w_i^{(0)}, \mathbf{M}_{j'} \rangle + \langle v_i^{(0)}, \mathbf{H}_{j'} \rangle \right) \\ &+ \frac{(a+b+c)^t - (a+b-c)^t}{4} \left( \langle w_i^{(0)}, \mathbf{M}_j \rangle + \langle v_i^{(0)}, \mathbf{H}_j \rangle \right) \end{aligned} \tag{33}$$

This matrix representation highlights the interactions between the alignment of true and spurious features during SGD updates. The diagonal elements $a$ dominate the contribution from existing alignments, while the off-diagonal terms $b, c$ capture the mutual influence between paired features and spurious alignments. Note that if $c$ is very small, it indicates that the spurious alignment $(j')$ has minimal influence, allowing $w_i$ to focus on learning purified features. Conversely, if $c$ is large, the spurious alignment could significantly interfere with the learning process, hindering the purification of features. The error term $Err_t$ accounts for higher-order noise or unmodeled effects in the update process.

Assuming a single spurious feature is a simplification for presentation that was made for ease of presentation in the proof and can be extended to a more general setting without altering the underlying insights. If each feature $j$ has $K-1$ spurious correlates, (31) becomes a $2K \times 2K$ matrix, and $N_i = j, j'$ in the last sentence of Theorem 4 contains $j$ and other $K-1$ features. Our analysis relies on the total spurious feature probability (bounded by $C_s$), not the number of correlated features, so **as long as the sum of all spurious feature probabilities is upper bounded by $C_s$, the core mechanism and insights of the theorem remain unchanged.**

### B.5. Zero-Shot Generalization on Image Classification

We consider an out-of-domain (OOD) setting for testing images and text prompts as follows.

**Image:** Each test image $x$ can be approximated by a sparse coding model with dictionary $\mathbf{M}'$,

$$x = \mathbf{M}' z'_x + \xi_x, \quad \|z'_x\|_0 = \Theta(1), \quad \|z'_x\|_{\max} = \Theta(1), \tag{34}$$

where $\mathbf{M}' = \mathbf{M}\mathbf{P}_1$, and $\max_{i,j} |(\mathbf{P}_1)_{ij} - \delta_{ij}| \le O(1/\sqrt{d})$ . The noise $\xi_x$ matches the training distribution (Assumption 1(d)) and $\delta_{ij}$ denotes the Kronecker delta function.

**Text:** Each class $k \in [K]$ has a prompt that has a sparse decomposition

$$y_k = \mathbf{H} z'_{y_k} + \xi_{y_k}, \quad \|z'_{y_k}\|_0 = \Theta(1), \quad \|z'_{y_k}\|_{\max} = \Theta(1). \tag{35}$$

If $x$ belongs to class $k$, then among all $K$ binary vectors $z'_{y_{k'}}$, $z'_x$ is maximally aligned with $z'_{y_k}$,

$$\|(z'_x)^\top z'_{y_k}\|_2 > \|(z'_x)^\top z'_{y_{k'}}\|_2, \quad \forall k' \neq k \tag{36}$$

This formulation reflects the intuition that $x$ belongs to class $k$ if its sparse representation is most similar to the sparse representation of class $k$'s text prompt.

## Appendix C. Technical Lemmas

**Definition 12 (Neuron Characterization)** *Let us define a few notations to characterize each neuron $w_i^{(t)}$'s behavior. For every constant $c_0 \in (0,1)$ and $\gamma \in (0, 0.1)$, by choosing $c_1 = 2+2(1-\gamma)c_0$ and $c_2 = \gamma c_0$, we define:*

*1. Let $\mathcal{S}^{(t)}_{j,sure} \subseteq [m]$ be those neurons $i \in [m]$ satisfying*

- $(\frac{1}{n}\sum_{i=1}^n \langle w_i^{(t)}, \mathbf{M}_j \rangle)^2 \ge \frac{(c_1+c_2)\log d}{d} \|\mathbf{M}\mathbf{M}^\top w_i^{(t)}\|_2^2$
- $(\frac{1}{n}\sum_{i=1}^n \langle w_i^{(t)}, \mathbf{M}_{j'} \rangle)^2 < \frac{(c_1-c_2)\log d}{d} \|\mathbf{M}\mathbf{M}^\top w_i^{(t)}\|_2^2$

*2. Let $\mathcal{S}^{(t)}_{j,pot} \subseteq [m]$ be those neurons $i \in [m]$ satisfying*

- $\langle w_i^{(t)}, \mathbf{M}_j \rangle^2 \geq \frac{(c_1 - c_2)\log d}{d} \|\mathbf{M}\mathbf{M}^\top w_i^{(t)}\|_2^2$

**Lemma 13 (Geometry at initialization)** *We initialize the parameters by $w_i^{(0)} \sim \mathcal{N}(0, \sigma_0^2 \mathbf{I}_{d_1})$, where $\sigma_0^2 = \Theta\left(\frac{1}{d_1 poly(d)}\right)$. We have with probability $\geq 1 - o(1/d^3)$ over the random initialization, for all $j \in [d]$:*

$$\left|\mathcal{S}_{j,sure}^{(0)}\right| = \Omega\left(d^{\frac{\gamma}{4}c_0}\right) =: \Xi_1$$
$$\left|\mathcal{S}_{j,pot}^{(0)}\right| \leq O\left(d^{2\gamma c_0}\right) =: \Xi_2$$

**Proof** If $g$ is standard Gaussian, then for every $t > 0$,

$$\frac{1}{\sqrt{2\pi}} \frac{(t)}{t^2+1} e^{-t^2/2} < \Pr_{g \sim \mathcal{N}(0,1)}[g > t] < \frac{1}{\sqrt{2\pi}} \frac{1}{(t)} e^{-t^2/2}. \tag{37}$$

We initialize the parameters by $w_i^{(0)} \sim \mathcal{N}(0, \sigma_0^2 \mathbf{I}_{d_1})$, where $\sigma_0^2 = \Theta\left(\frac{1}{d_1 \mathrm{poly}(d)}\right)$. We have $\frac{1}{n}\sum_{i=1}^n \langle w_i^{(0)}, \mathbf{M}_i \rangle \sim \mathcal{N}\left(0, \frac{\sigma_0^2}{n}\right)$.

Therefore, for every $i \in m$ and $j \in d$, we have

$$\begin{aligned} p_1 &= \Pr\left[\left(\frac{1}{n}\sum_{i=1}^n \langle w_i^{(0)}, \mathbf{M}_j \rangle\right)^2 \geq (c_1 + c_2)\frac{\sigma_0^2}{n}\log d\right] \\ &= \Theta\left(\frac{1}{\log d}\right) \cdot \frac{1}{d^{(c_1+c_2)/2}} \\ &= \Theta\left(\frac{1}{\sqrt{\log d}}\right) \cdot \frac{1}{d \cdot d^{(1-\gamma/2)c_0}} \end{aligned} \tag{38}$$

$$\begin{aligned} p_2 &= \Pr\left[\left(\frac{1}{n}\sum_{i=1}^n \langle w_i^{(0)}, \mathbf{M}_{j'} \rangle\right)^2 \geq (c_1 - c_2)\frac{\sigma_0^2}{n}\log d\right] \\ &= \Theta\left(\frac{1}{\log d}\right) \cdot \frac{1}{d^{(c_1-c_2)/2}} \\ &= \Theta\left(\frac{1}{\sqrt{\log d}}\right) \cdot \frac{1}{d \cdot d^{(1-3\gamma/2)c_0}} \end{aligned} \tag{39}$$

Let $\mathcal{S}_{j,\text{sure}}^{(0)} \subseteq [m]$ be those neurons $i \in [m]$ satisfying

- $(\frac{1}{n}\sum_{i=1}^n \langle w_i^{(0)}, \mathbf{M}_j \rangle)^2 \geq \frac{(c_1+c_2)\log d}{d} \|\mathbf{M}\mathbf{M}^\top w_i^{(0)}\|_2^2$
- $(\frac{1}{n}\sum_{i=1}^n \langle w_i^{(0)}, \mathbf{M}_{j'} \rangle)^2 < \frac{(c_1-c_2)\log d}{d} \|\mathbf{M}\mathbf{M}^\top w_i^{(0)}\|_2^2$

By concentration with respect to all $m$ choices of $i \in [m]$, we know with probability at least $1 - o\left(\frac{1}{d^3}\right)$ it satisfies $\left|\mathcal{S}_{j,\text{sure}}^{(0)}\right| = \Omega\left(d^{\frac{\gamma}{4}c_0}\right)$.

Let $\mathcal{S}_{j,\text{pot}}^{(0)} \subseteq [m]$ be those neurons $i \in [m]$ satisfying

- $\langle w_i^{(0)}, \mathbf{M}_j \rangle^2 \geq \frac{(c_1 - c_2)\log d}{d} \|\mathbf{M}\mathbf{M}^\top w_i^{(0)}\|_2^2$

By concentration with respect to all $m$ choices of $i \in [m]$, we know with probability at least $1 - o\left(\frac{1}{d^3}\right)$ it satisfies $\left|\mathcal{S}^{(0)}_{j,\text{pot}}\right| = O\left(d^{2\gamma c_0}\right)$.

More details of the proof can be found in Lemma B.2 of [1]. ■

**Lemma 14** *With high probability $1 - \frac{1}{poly(d)}$, for every $i \in [m]$, the following holds:*

$$\Pr\left[\left(\frac{1}{2n}\sum_{i=1}^{n}\langle w_i^{(0)}, \mathbf{M}_j\rangle - \langle w_i^{(0)}, \mathbf{M}_{j'}\rangle\right)^2 \geq \frac{1}{d}\frac{\sigma_0^2}{2n}\log d\right] \geq 1 - O\left(\frac{1}{\sqrt{d}}\right) \tag{40}$$

**Lemma 15** *With high probability $1 - \frac{1}{poly(d)}$, for every $i \in [m]$, the following holds:*

$$\|\mathbf{M}\mathbf{M}^\top w_i^{(0)}\|_2^2 + \|\mathbf{H}\mathbf{H}^\top v_i^{(0)}\|_2^2 \in 2d\sigma_0^2\left[1 - \widetilde{O}\left(\frac{1}{\sqrt{d}}\right), 1 + \widetilde{O}\left(\frac{1}{\sqrt{d}}\right)\right]. \tag{41}$$

**Proof** Let $X \sim \chi_n^2$. By standard properties of the chi-squared distribution, we know that with probability at least $1-\delta$,

$$|X - n| \leq 2\sqrt{n\log(1/\delta)}. \tag{42}$$

In our case, we consider $\frac{\|\mathbf{M}\mathbf{M}^\top w_i^{(0)}\|_2^2 + \|\mathbf{H}\mathbf{H}^\top v_i^{(0)}\|_2^2}{\sigma_0^2} \sim \chi_{2d}^2$. Setting $\delta = \frac{1}{\text{poly}(d)}$, we have $n = 2d$, and thus, with high probability $1 - \frac{1}{\text{poly}(d)}$, the following holds:

$$\left|\frac{\|\mathbf{M}\mathbf{M}^\top w_i^{(0)}\|_2^2 + \|\mathbf{H}\mathbf{H}^\top v_i^{(0)}\|_2^2}{\sigma_0^2} - 2d\right| \leq 2\sqrt{2d\log(\text{poly}(d))}. \tag{43}$$

Rearranging and incorporating the scaling factor $\sigma_0^2$, we get:

$$\|\mathbf{M}\mathbf{M}^\top w_i^{(0)}\|_2^2 + \|\mathbf{H}\mathbf{H}^\top v_i^{(0)}\|_2^2 \in 2d\sigma_0^2\left[1 - \widetilde{O}\left(\frac{1}{\sqrt{d}}\right), 1 + \widetilde{O}\left(\frac{1}{\sqrt{d}}\right)\right]. \tag{44}$$

■

**Lemma 16 (Noise Projection Bound)** *For the spurious dense noise $\xi_{x_p} \sim \mathcal{N}(0, \sigma_\xi^2 \mathbf{I}_{d_1})$, where the variance satisfies $\omega\left(\frac{1}{d_1}\right) \leq \sigma_\xi^2 \leq O\left(\frac{1}{d}\right)$, the following holds with high probability $1 - e^{-\Omega(d_1)}$:*

$$|\langle w_i, \xi\rangle|^2 \leq O\left(\frac{\|w_i\|_2^2}{d^{1+c_0}}\right), \quad \forall i \in [m]. \tag{45}$$

**Proof** For all $j \in [d_1]$, by the properties of the Gaussian distribution, we have:

$$\Pr_{\xi}\left[\langle \mathbf{M}_j, \xi\rangle^2 \leq O\left(\frac{1}{d^{1+c_0}}\right)\right] \geq 1 - e^{-\Omega(d_1)}. \tag{46}$$

Now, consider the term $|\langle w_i, \xi\rangle|^2$. We decompose it as:

$$|\langle w_i, \xi\rangle|^2 = \sum_{j\in[d]} |\langle w_i, \mathbf{M}_j\rangle|^2 \cdot |\langle \mathbf{M}_j, \xi\rangle|^2 + \sum_{j\in[d_1]\setminus[d]} |\langle w_i, \mathbf{M}_j^\perp\rangle|^2 \cdot |\langle \mathbf{M}_j^\perp, \xi\rangle|^2. \tag{47}$$

For the first term, since $|\langle \mathbf{M}_j, \xi \rangle|^2 \leq O\left(\frac{1}{d^{1+c_0}}\right)$ with high probability, we have:

$$\sum_{j\in[d]} |\langle w_i, \mathbf{M}_j \rangle|^2 \cdot |\langle \mathbf{M}_j, \xi \rangle|^2 \leq \sum_{j\in[d]} O\left(\frac{|\langle w_i, \mathbf{M}_j \rangle|^2}{d^{1+c_0}}\right). \tag{48}$$

Similarly, for the second term:

$$\sum_{j\in[d_1]\setminus[d]} |\langle w_i, \mathbf{M}_j^{\perp} \rangle|^2 \cdot |\langle \mathbf{M}_j^{\perp}, \xi \rangle|^2 \leq \sum_{j\in[d_1]\setminus[d]} O\left(\frac{|\langle w_i, \mathbf{M}_j^{\perp} \rangle|^2}{d^{1+c_0}}\right). \tag{49}$$

Combining these, we have:

$$|\langle w_i, \xi \rangle|^2 \leq O\left(\frac{\|\mathbf{M}\mathbf{M}^\top w_i\|_2^2}{d^{1+c_0}} + \frac{\|\mathbf{M}^{\perp}\mathbf{M}^{\perp\top} w_i\|_2^2}{d^{1+c_0}}\right). \tag{50}$$

Since $\|\mathbf{M}\mathbf{M}^\top w_i\|_2^2 + \|\mathbf{M}^{\perp}\mathbf{M}^{\perp\top} w_i\|_2^2 = \|w_i\|_2^2$, we conclude:

$$|\langle w_i, \xi \rangle|^2 \leq O\left(\frac{\|w_i\|_2^2}{d^{1+c_0}}\right). \tag{51}$$

Thus, the lemma holds. ∎

**Lemma 17 (Tail Bound for Matrix Product)** *Let $\mathbf{Q} \in \mathbb{R}^{n\times n}$ be a symmetric matrix, and let $w, v$ be independent zero-mean Gaussian random vectors with covariance matrix $\mathbf{I}_n$. Define*

$$Z := \sum_{i,j=1}^{n} Q_{ij} w_i v_j. \tag{52}$$

*Then, for any $\delta > 0$, the following tail bound holds:*

$$\Pr[|Z| \geq \delta] \leq 4\exp\left(-\frac{\delta^2}{4\|\mathbf{Q}\|_F^2 + 4\delta\|\mathbf{Q}\|_{op}}\right). \tag{53}$$

**Lemma 18 (Bound Inner Product)** *Consider the inner product between the feature vectors at initialization:*

$$\langle f(x), h(y) \rangle = \langle \mathbf{W}x, \mathbf{V}y \rangle = \sum_{l=1}^{m} w_l^\top x y^\top v_l = \sum_{l=1}^{m} \sum_{i,j=1}^{d_1} (x_i^\top y_j) w_l^\top v_l. \tag{54}$$

*Here, using Lemma 17, $\mathbf{Q} = xy^\top$, with $\|\mathbf{Q}\|_{op} = \Theta(1)$, $\|\mathbf{Q}\|_F = \Theta(1)$ and $\sigma_0^2 = \Theta\left(\frac{1}{d_1 poly(d)}\right)$. Then, at initialization ($t = 0$), the following holds:*

$$\Pr[|\langle f^{(t)}(x), h^{(t)}(y) \rangle| \geq \Omega(1)] \leq e^{-poly(d)}, \tag{55}$$

**Lemma 19 (Concentration bound for empirical loss and gradients)** *There exist $N \geq poly(d)$ for some sufficiently large polynomial and all $\|w_i\|_2 \leq O(d)$, $i \in [m]$ , it satisfies*

$$\left| \frac{1}{N} \sum_{p \in [N]} L(f^{(t)}, h^{(t)}; (x_p, y_p)) - \mathbb{E}_{(x_p, y_p) \in D}[L(f^{(t)}, h^{(t)}; (x_p, y_p))] \right| \leq O(\frac{1}{d}) \tag{56}$$

$$\left\| \frac{1}{N} \sum_{p \in [N]} \nabla_{w_i} L(f^{(t)}, h^{(t)}; (x_p, y_p)) - \mathbb{E}_{(x_p, y_p) \in D}[\nabla_{w_i} L(f^{(t)}, h^{(t)}; (x_p, y_p))] \right\|_2 \leq O(\frac{1}{d}) \tag{57}$$

**Proof** The proof can be done by trivial VC dimension or Rademacher complexity arguments similarly to Lemma A.2. [1]. ■

**Lemma 20 (Misalignment Probability Bound)** *The probability of spurious alignment satisfies:*

$$\frac{\log\left(\frac{1}{2\gamma c_0}\right)}{2\log\frac{d_1}{d}} < \Pr(|z_{y_p}^j| = 1 \mid |z_{x_p}^{j'}| = 1) < \frac{1}{2}. \tag{58}$$

**Proof** By concentration over all $m$ choices of $i \in [m]$, we find that with probability at least $1-o\left(\frac{1}{d^3}\right)$, the number of neurons satisfying:

$$\left(\frac{1}{n}\sum_{i=1}^{n}\langle w_i, \mathbf{M}_j\rangle\right)^2 < (c_1 + 4c_2)\frac{\sigma_0^2}{n}\log d \tag{59}$$

is $o(1)$.

In addition, for all neurons, we have:

$$\max\left(\langle w_i^{(T_1)}, \mathbf{M}_{j'}\rangle^2\right) \leq \frac{c_1 + 3c_2}{2}\frac{\log d}{d} \cdot \frac{\|w_i^{(T_1)}\|_2^2 + \|v_i^{(T_1)}\|_2^2}{2}. \tag{60}$$

Define:

$$\Delta^{(T_1)} = \frac{(a+b-c)^{T_1}}{4}\left|\langle w_i^{(0)}, \mathbf{M}_j\rangle + \langle v_i^{(0)}, \mathbf{H}_j\rangle - \langle w_i^{(0)}, \mathbf{M}_{j'}\rangle - \langle v_i^{(0)}, \mathbf{H}_{j'}\rangle\right|. \tag{61}$$

Thus:

$$\langle w_i^{(T_1)}, \mathbf{M}_{j'}\rangle^2 = \left|\max\left(\langle w_i^{(T_1)}, \mathbf{M}_{j'}\rangle\right) - \Delta^{(T_1)}\right|^2 \geq \frac{c_1 - c_2}{2}\frac{\log d}{d} \cdot \frac{\|w_i^{(T_1)}\|_2^2 + \|v_i^{(T_1)}\|_2^2}{2}. \tag{62}$$

We begin by expressing $a+b-c$ and $a+b+c$ as functions of $P_1 = \Pr(|z_{y_p}^j| = 1 \mid |z_{x_p}^{j'}| = 1)$ and $P_2 = \Pr(|z_{y_p}^j| = 1 \mid |z_{x_p}^j| = 1)$, where $P_1 + P_2 = 1$:

$$a+b-c = 1 - \eta\lambda + \eta\frac{(P_1 - P_2)C_z\log\log d}{d}, \tag{63}$$

$$a+b+c=1-\eta\lambda+\eta\frac{(P_1+P_2)C_z\log\log d}{d}. \tag{64}$$

Using Eq (62), Eq (32) and Eq (33), we derive:

$$\frac{(a+b-c)^{2T_1}}{(a+b+c)^{2T_1}} \le \left(\sqrt{\frac{c_1+3c_2}{2}}-\sqrt{\frac{c_1-c_2}{2}}\right)^2 \le 2c_2^2. \tag{65}$$

Substituting back, we find:

$$\frac{\log\left(\frac{1}{2\gamma c_0}\right)}{2\log\frac{d_1}{d}} < P_1 < \frac{1}{2}. \tag{66}$$

For example, setting $c_0=0.1$, $\gamma=0.005$, $d=100$, and $d_1=10000$, we calculate:

$$\frac{1}{4} \le \Pr(|z^j_{y_p}|=1 \mid |z^{j'}_{x_p}|=1) < \frac{1}{2}. \tag{67}$$

This concludes the proof by bounding $\Pr(|z^j_{y_p}|=1 \mid |z^{j'}_{x_p}|=1)$ under the given conditions. ■

## Appendix D. ITCP on Raw Data I

In this section we analyze Phase I of ITCP on Raw Data as the training iterations $t \le T_1$, where $T_1=\Theta\left(\frac{d\log d}{\eta}\right)$ is the iteration when all $\frac{\|w_i^{(T_1)}\|_2^2+\|v_i^{(T_1)}\|_2^2}{2} \ge \|w_i^{(0)}\|_2^2+\|v_i^{(0)}\|_2^2$. When $t\le T_1$, we set $b_i^{(t)}=0$. For every neuron $i\in[m]$, the weights $w_i$ and $v_i$ exhibit an increase in alignment along the direction of informative features $\mathbf{M}$ and $\mathbf{H}$, while showing negligible increase in alignment along the direction of noise features $\mathbf{M}^\perp$ and $\mathbf{H}^\perp$.

Based on subsection B.2, we have $\Pr(|z^j_{y_p}|=1 \mid |z^{j'}_{x_p}|=1)=\Theta(1)$, so $\mathbb{E}\left[z^j_x z^j_y\right]$ and $\mathbb{E}\left[z^j_x z^{j'}_y\right]$ both in $\Theta\left(\frac{1}{d}\right)$. In this case, $w_i^{(t+1)}$ is jointly influenced by $\mathbf{M}_j$ and $\mathbf{M}_{j'}$, with both features contributing comparably to the updates.

To simplify our analysis, we consider the worse case where $\Pr(|z^{j'}_{y_p}|=1 \mid |z^j_{x_p}|=1) = \Pr(|z^j_{y_p}|=1 \mid |z^j_{x_p}|=1)=\frac{1}{2}$ such that $\mathbb{E}\left[z^j_x z^j_y\right]=\mathbb{E}\left[z^j_x z^{j'}_y\right]=\frac{C_z}{2d}$, so using Eq (32), Eq (33) and $b_i^{(t)}=0$, we have

$$\langle w_i^{(t)},\mathbf{M}_j\rangle=\frac{(a+b+c)^t}{4}\left(\langle w_i^{(0)},\mathbf{M}_j\rangle+\langle v_i^{(0)},\mathbf{H}_j\rangle+\langle w_i^{(0)},\mathbf{M}_{j'}\rangle+\langle v_i^{(0)},\mathbf{H}_{j'}\rangle\right) \tag{68}$$

$$\langle w_i^{(t)},\mathbf{M}_{j'}\rangle=\frac{(a+b+c)^t}{4}\left(\langle w_i^{(0)},\mathbf{M}_j\rangle+\langle v_i^{(0)},\mathbf{H}_j\rangle+\langle w_i^{(0)},\mathbf{M}_{j'}\rangle+\langle v_i^{(0)},\mathbf{H}_{j'}\rangle\right) \tag{69}$$

This represents the worst-case scenario as the contributions of the aligned feature $\mathbb{E}\left[z^j_x z^j_y\right]$ and the spurious feature $\mathbb{E}\left[z^j_x z^{j'}_y\right]$ are identical. Under real circumstances, we expect $\mathbb{E}\left[z^j_x z^j_y\right] < \mathbb{E}\left[z^j_x z^{j'}_y\right]$, which would result in $\langle w_i^{(t+1)},\mathbf{M}_j\rangle > \langle w_i^{(t+1)},\mathbf{M}_{j'}\rangle$. However, in this worst-case scenario, the equality of contributions prevents the network from prioritizing purified features, resulting in equal magnitudes for $\langle w_i^{(t+1)}, \mathbf{M}_j \rangle$ and $\langle w_i^{(t+1)}, \mathbf{M}_{j'} \rangle$, thereby hindering effective feature separation.

We first provide a lower bound for $\|\mathbf{M}\mathbf{M}^\top w_i^{(t)}\|_2^2$ for iterations $t \le t_1$. From Eq (122) and Eq (69) we have:

$$
\begin{aligned}
\|\mathbf{M}\mathbf{M}^\top w_i^{(t)}\|_2^2 &= \sum_{i=1}^{d} \left[ \frac{(a+b+c)^t}{4} \left( \langle w_i^{(0)}, \mathbf{M}_j \rangle + \langle v_i^{(0)}, \mathbf{H}_j \rangle \right) + \frac{(a+b+c)^t}{4} \left( \langle w_i^{(0)}, \mathbf{M}_{j'} \rangle + \langle v_i^{0}, \mathbf{H}_{j'} \rangle \right) \right]^2 \\
&= \left(1 + \frac{\eta C_z}{d}\right)^{2t} \frac{\|\mathbf{M}\mathbf{M}^\top w_i^{(0)}\|_2^2 + \|\mathbf{H}\mathbf{H}^\top v_i^{(0)}\|_2^2}{8}
\end{aligned} \tag{70}
$$

$$
\|\mathbf{M}^\perp (\mathbf{M}^\perp)^\top w_i^{(t)}\|_2^2 \le \left(1 + \frac{1}{\text{poly}(d)}\right) \|\mathbf{M}^\perp (\mathbf{M}^\perp)^\top w_i^{(0)}\|_2^2. \tag{71}
$$

The detailed proof of Eq (71) can be found in Hypothesis C.4 of [24].

A similar result holds for $\|\mathbf{H}\mathbf{H}^\top v_i^{(t)}\|_2^2$ and $\|\mathbf{H}^\perp (\mathbf{H}^\perp)^\top v_i^{(t)}\|_2^2$.

Eq (70) and Eq (71) shows that the image and text dictionary features $\mathbf{M}, \mathbf{H}$ can grow exponentially, while the noisy features $\mathbf{M}^\perp, \mathbf{H}^\perp$ remain almost unchanged when $t \le T_1$.

For $\mathbf{M}_j^\perp$ where $j \in [d_1] \setminus [d]$, using Eq (71), we obtain:

$$
|\langle w_i^{(t+1)}, \mathbf{M}_j^\perp \rangle|^2 \le O\left(\frac{1}{d_1}\right) \|w_i^{(0)}\|_2^2 \le O\left(\frac{1}{d_1}\right) \cdot \frac{\|w_i^{(T_1)}\|_2^2 + \|v_i^{(T_1)}\|_2^2}{2}. \tag{72}
$$

This result demonstrates that the noisy features $\mathbf{M}_j^\perp$ experience nearly no increase during this phase, remaining insignificant in their contribution to the alignment of $w_i$.

### D.1. Lower Bound of Alignment for $i \in S_{j,\text{sure}}$

This section provides a analysis of the alignment growth for neurons $i \in S_{j,\text{sure}}$. Specifically, we demonstrate that for every $j \in [d]$, if $i \in S_{j,\text{sure}}$, the alignment $\langle \mathbf{M}_j, w_i^{(t)} \rangle^2$ and its spurious alignment $\langle \mathbf{M}'_j, w_i^{(t)} \rangle^2$ increase exponentially when $t \le T_1$.

We now prove the lower bound of $|\langle w_i^{(T_1)}, \mathbf{M}_j \rangle|^2$ for $i \in S_{j,\text{sure}}$:

$$
\begin{aligned}
|\langle w_i^{(T_1)}, \mathbf{M}_j \rangle|^2 &= \left(1 + \eta \frac{C_z}{d}\right)^{2T_1} \left( \frac{\langle w_i^{(0)}, \mathbf{M}_j \rangle + \langle v_i^{(0)}, \mathbf{H}_{j'} \rangle + \langle w_i^{(0)}, \mathbf{M}_{\mathbf{j}'} \rangle + \langle v_i^{(0)}, \mathbf{H}_j \rangle}{4} \right)^2 \\
&\overset{\diamondsuit}{\ge} \left(1 + \eta \frac{C_z}{d}\right)^{2T_1} \cdot \frac{(c_1 + c_2) \log d}{d} \cdot \frac{\|\mathbf{M}\mathbf{M}^\top w_i^{(0)}\|_2^2 + \|\mathbf{H}\mathbf{H}^\top v_i^{(0)}\|_2^2}{8} \\
&\overset{\heartsuit}{=} \frac{(c_1 + c_2) \log d}{d} \cdot \frac{\|\mathbf{M}\mathbf{M}^\top w_i^{(T_1)}\|_2^2 + \|\mathbf{H}\mathbf{H}^\top v_i^{(T_1)}\|_2^2}{2} \\
&\overset{\clubsuit}{\ge} \frac{(c_1 + c_2) \log d}{d} \cdot \frac{\|w_i^{(T_1)}\|_2^2 + \|v_i^{(T_1)}\|_2^2 - \|w_i^{(0)}\|_2^2 - \|v_i^{(0)}\|_2^2}{2} \\
&\overset{\spadesuit}{>} \frac{(1 + c_0 - \gamma c_0) \log d}{d} \cdot \frac{\|w_i^{(T_1)}\|_2^2 + \|v_i^{(T_1)}\|_2^2}{2}
\end{aligned} \tag{73}
$$

In $\diamondsuit$ we use Definition 12. In $\heartsuit$ we use Eq (70). In $\clubsuit$ we use $\frac{\|w_i^{(T_1)}\|_2^2+\|v_i^{(T_1)}\|_2^2}{2} \geq \|w_i^{(0)}\|_2^2 + \|v_i^{(0)}\|_2^2$. In $\spadesuit$ we use $c_1 + c_2 > 2(1 + c_0 - \gamma c_0)$.

Similarly, $|\langle w_i^{(T_1)}, \mathbf{M}_{j'}\rangle|^2$ have the same lower bound.

## D.2. Upper Bound of Alignment for $i \notin S_{j,\text{pot}}$

In this subsection, we analyze the alignment of neuron $i \notin S_{j,\text{pot}}$ with the feature $\mathbf{M}_j$ and provide an upper bound for $|\langle w_i^{(T_1)}, \mathbf{M}_j\rangle|^2$. While neurons $i \notin S_{j,\text{pot}}$ still exhibit exponential growth in their alignment, their weaker initialization results in significantly smaller alignment compared to neurons in $S_{j,\text{sure}}$, limiting their contribution to learning the feature $\mathbf{M}_j$.

To establish the bound, we begin with the following expression:

$$
\begin{aligned}
|\langle w_i^{(T_1)}, \mathbf{M}_j\rangle|^2 &= \left(1+\eta\frac{C_z}{d}\right)^{2T_1}\left(\frac{\langle w_i^{(0)}, \mathbf{M}_j\rangle + \langle v_i^{(0)}, \mathbf{H}_{j'}\rangle + \langle w_i^{(0)}, \mathbf{M}_{\mathbf{j}'}\rangle + \langle v_i^{(0)}, \mathbf{H}_j\rangle}{4}\right)^2 \\
&\overset{\diamondsuit}{\leq} \left(1+\eta\frac{C_z}{d}\right)^{2T_1} \cdot \frac{(c_1-c_2)\log d}{d} \cdot \frac{\|\mathbf{M}\mathbf{M}^\top w_i^{(0)}\|_2^2 + \|\mathbf{H}\mathbf{H}^\top v_i^{(0)}\|_2^2}{8} \\
&= \frac{(c_1-c_2)\log d}{d} \cdot \frac{\|\mathbf{M}\mathbf{M}^\top w_i^{(T_1)}\|_2^2 + \|\mathbf{H}\mathbf{H}^\top v_i^{(T_1)}\|_2^2}{2}.
\end{aligned}
\tag{74}
$$

Here, in $\diamondsuit$, we use Lemma 12, which captures the reduced alignment for neurons outside $S_{j,\text{pot}}$.

Similar to the analysis for $i \in S_{j,\text{sure}}$, the alignment strength for $i \notin S_{j,\text{pot}}$ is weaker, as $c_1 - c_2$ is less than $2(1 + c_0 - \gamma c_0)$, leading to:

$$
|\langle w_i^{(T_1)}, \mathbf{M}_j\rangle|^2 < \frac{(1+c_0-3\gamma c_0)\log d}{d} \cdot \frac{\|w_i^{(T_1)}\|_2^2 + \|v_i^{(T_1)}\|_2^2}{2}. \tag{75}
$$

This inequality highlights the slower alignment for neurons outside $S_{j,\text{pot}}$, distinguishing their behavior from neurons in $S_{j,\text{sure}}$. Consequently, $i \notin S_{j,\text{pot}}$ contributes less significantly to the alignment of $\mathbf{M}_j$, reinforcing the importance of initial affinity for effective alignment.

## D.3. Summary

At this stage ($t \leq T_1$), we do not consider the worst-case scenario where the probability bounds for feature coupling satisfy

$$
\frac{\log(1/c_0)}{2\log d} < \Pr(|z_{y_p}^{j'}| = 1 \mid |z_{x_p}^{j}| = 1) < \frac{1}{2} < \Pr(|z_{y_p}^{j}| = 1 \mid |z_{x_p}^{j}| = 1) < 1
$$

(as assumed in SubSection B.2). Thus, we summarize the results when $t \leq T_1$ as follows:

1. For $i \in S_{j,\text{sure}}$, the alignment strength satisfies:

$$
|\langle w_i^{(T_1)}, \mathbf{M}_j\rangle|^2 > |\langle w_i^{(T_1)}, \mathbf{M}_{j'}\rangle|^2 > \frac{(1+c_0-\gamma c_0)\log d}{d} \cdot \frac{\|w_i^{(T_1)}\|_2^2 + \|v_i^{(T_1)}\|_2^2}{2}, \tag{76}
$$

where $j'$ represents the corresponding spurious alignment feature.

2. For $i \notin S_{j,\text{pot}}$, the alignment strength satisfies:

$$|\langle w_i^{(T_1)}, \mathbf{M}_j \rangle|^2 < \frac{(1 + c_0 - 3\gamma c_0)\log d}{d} \cdot \frac{\|w_i^{(T_1)}\|_2^2 + \|v_i^{(T_1)}\|_2^2}{2}. \tag{77}$$

3. For $\mathbf{M}_j^{\perp}$ where $j \in [d_1] \setminus [d]$, we have:

$$|\langle w_i^{(t+1)}, \mathbf{M}_j^{\perp} \rangle|^2 < O\left(\frac{1}{d_1}\right) \cdot \frac{\|w_i^{(T_1)}\|_2^2 + \|v_i^{(T_1)}\|_2^2}{2}. \tag{78}$$

These results demonstrate that when $t \leq T_1$, all features in $\mathbf{M}$ increase, but the alignment for $i \in S_{j,\text{sure}}$, including the corresponding spurious alignment, grows significantly larger due to favorable initialization. In contrast, noisy features $\mathbf{M}^{\perp}$ remain unchanged.

## Appendix E. ITCP on Raw Data II

The Phase II of ITCP on Raw Data is defined as the training iterations $T_1 < t \leq T_2$, where $T_2 - T_1 = \Theta\left(\frac{d \log d}{\eta}\right)$.

At the beginning of this phase, we set the bias threshold as:

$$b_i^{(T_1)} = \sqrt{\frac{(1 + c_0 - 2\gamma c_0)\log d}{d} \cdot \frac{\|w_i^{(T_1)}\|_2^2 + \|v_i^{(T_1)}\|_2^2}{2}}. \tag{79}$$

During training, the bias threshold is iteratively updated as:

$$b_i^{(t+1)} = \left(1 + \frac{\eta}{d}\right) b_i^{(t)}, \tag{80}$$

until all neurons satisfy:

$$\|w_i^{(T_2)}\|_2^2 \geq \Omega(d) \|w_i^{(T_1)}\|_2^2. \tag{81}$$

In this phase, the dynamics of alignment vary depending on whether a neuron belongs to $S_{j,\text{sure}}$ or not:

- For $i \notin S_{j,\text{pot}}$: The weights $w_i$ and $v_i$ show negligible alignment growth with both the informative features $\mathbf{M}_j$, $\mathbf{H}_j$ and the noise features $\mathbf{M}^{\perp}$, $\mathbf{H}^{\perp}$. This is due to their weaker initialization, as shown in Phase I, and the effect of the indicator function when $t \geq T_1$ which prevents them from being activated. As a result, their capacity to learn meaningful alignments during this phase is significantly limited.

- For $i \in S_{j,\text{sure}}$: The weights $w_i$ and $v_i$ exhibit continued alignment growth with the informative features $\mathbf{M}_j$, $\mathbf{H}_j$. Additionally, their alignment with the corresponding spurious features $\mathbf{M}_{j'}$, $\mathbf{H}_{j'}$ also increases due to their strong initialization, as shown in Phase I, and the effect of the indicator function when $t \geq T_1$, which ensures they are always activated.

By the end of this stage ($t = T_2$), the weights $w_i$, $v_i$ will predominantly focus on the features $\mathbf{M}_j$, $\mathbf{H}_j$ if $i \in S_{j,\text{sure}}$, while largely ignoring the features $\mathbf{M}_j$, $\mathbf{H}_j$ if $i \notin S_{j,\text{pot}}$, as well as the noise features $\mathbf{M}^{\perp}$, $\mathbf{H}^{\perp}$. This separation lays the foundation for the Phase II of ITCP on Raw Data, where spurious alignments are expected to further diminish due to the dominance of true feature alignments.

Similarly to the proof of $t \leq T_1$ To simplify our analysis, we still consider the worse case where $\Pr(|z_{y_p}^{j'}| = 1 \mid |z_{x_p}^{j}| = 1) = \Pr(|z_{y_p}^{j}| = 1 \mid |z_{x_p}^{j}| = 1) = \frac{1}{2}$ such that $\mathbb{E}\left[z_x^j z_y^j\right] = \mathbb{E}\left[z_x^j z_y^{j'}\right] = \frac{C_z}{2d}$.

### E.1. Alignment for $i \in S_{j,\text{sure}}$

This section provides a analysis of the alignment growth for neurons $i \in S_{j,\text{sure}}$. Specifically, we demonstrate that for every $j \in [d]$, if $i \in S_{j,\text{sure}}$, the alignment $\langle \mathbf{M}_j, w_i^{(t)} \rangle^2$ and its spurious alignment $\langle \mathbf{M}'_j, w_i^{(t)} \rangle^2$ increase exponentially when $T_1 < t \le T_2$.

For $i \in S_{j,\text{sure}}$, using Lemma 16, the following holds with high probability $1 - e^{-\Omega(d_1)}$ when $T_1 < t \le T_2$ :

$$\left| \langle w_i^{(t)}, \xi \rangle \right|^2 \le O\left( \frac{\left\| w_i^{(t)} \right\|_2^2}{d^{1+c_0}} \right) < b_i^{(t)} \tag{82}$$

Therefore, with high probability $1 - e^{-\Omega(d_1)}$, using Eq (76) and Eq (79) the indicator function satisfies the condition when $t = T_1$:

$$\mathbf{1}_{\left| \left\langle w_i^{(t)}, x_p \right\rangle \right| \ge b_i^{(t)}} \cdot \mathbf{1}_{\left| \left\langle v_i^{(t)}, y_p \right\rangle \right| \ge b_i^{(t)}} = 1, \tag{83}$$

we can ensure that:

$$\mathbb{E}\left[ z_x^j z_y^j \cdot \mathbf{1}_{\left| \left\langle w_i^{(t)}, x_p \right\rangle \right| \ge b_i^{(t)}} \cdot \mathbf{1}_{\left| \left\langle v_i^{(t)}, y_p \right\rangle \right| \ge b_i^{(t)}} \right] = \frac{C_z}{d}. \tag{84}$$

Using Eq (116) we know that $\left(1 + \eta \frac{C_z}{2d}\right) > \left(1 + \frac{\eta}{d}\right)$ and using Eq (31) we have

$$|\langle w_i^{(t+1)}, \mathbf{M}_j \rangle| > (1 + \frac{\eta}{d}) b_i^{(t)} = b_i^{(t+1)}. \tag{85}$$

This implies that when $t > T_1$, the alignment strength of informative features surpasses the updated bias threshold $b_i^{(t)}$. Consequently, the indicator functions become consistently activated $T_1 < t \le T_2$ such that

$$\mathbf{1}_{\left| \left\langle w_i^{(t)}, x_p \right\rangle \right| \ge b_i^{(t)}} \cdot \mathbf{1}_{\left| \left\langle v_i^{(t)}, y_p \right\rangle \right| \ge b_i^{(t)}} = 1, \tag{86}$$

Using Eq (31), the weight dynamics for $|\langle w_i^{(t+1)}, \mathbf{M}_j \rangle|$ can be expressed as when $T_1 < t \le T_2$:

$$|\langle w_i^{(t+1)}, \mathbf{M}_j \rangle| = \left(1 + \eta \frac{C_z}{d}\right) \left( \frac{\langle w_i^{(t)}, \mathbf{M}_j \rangle + \langle v_i^{(t)}, \mathbf{H}_{j'} \rangle + \langle w_i^{(t)}, \mathbf{M}_{\mathbf{j}}^{\perp} \rangle + \langle v_i^{(t)}, \mathbf{H}_j \rangle}{4} \right). \tag{87}$$

Similarly, $|\langle w_i^{(T_1)}, \mathbf{M}_{j'} \rangle|^2$ have the same result.

### E.2. Alignment for $i \notin S_{j,\text{pot}}$

In this section, we analyze the alignment behavior for neurons $i \notin S_{j,\text{pot}}$. Specifically, we demonstrate that for every $j \in [d]$, if $i \notin S_{j,\text{pot}}$, the alignment $\langle \mathbf{M}_j, w_i^{(t)} \rangle^2$ exhibits negligible growth during the interval $T_1 < t \le T_2$.

For $i \notin S_{j,\text{pot}}$, using Eq (156), Eq (79) and Eq (76), we have with high probability $1 - e^{-\Omega(d_1)}$, similarly to the proof of $i \in S_{j,\text{sure}}$, the indicator function satisfies the condition when $t = T_1$:

$$\mathbf{1}_{\left| \left\langle w_i^{(t)}, x_p \right\rangle \right| \ge b_i^{(t)}} \cdot \mathbf{1}_{\left| \left\langle v_i^{(t)}, y_p \right\rangle \right| \ge b_i^{(t)}} = 0, \tag{88}$$

We can ensure that:

$$\mathbb{E}\left[z_x^j z_y^j \cdot \mathbf{1}_{\left|\left\langle w_i^{(t)}, x_p\right\rangle\right| \geq b_i^{(t)}} \cdot \mathbf{1}_{\left|\left\langle v_i^{(t)}, y_p\right\rangle\right| \geq b_i^{(t)}}\right] \leq o\left(\frac{1}{d^2}\right). \tag{89}$$

Using Eq (116) we know that $\left(1+o(\frac{\eta}{d^2})\right) < \left(1+\frac{\eta}{d}\right)$ and using Eq (31) we have

$$|\langle w_i^{(t+1)}, \mathbf{M}_j\rangle| < (1+\frac{\eta}{d})b_i^{(t)} = b_i^{(t+1)}. \tag{90}$$

This implies that when $t > T_1$, the alignment strength of informative features does not surpass the updated bias threshold $b_i^{(t)}$. Consequently, the indicator functions become consistently not activated $T_1 < t \leq T_2$ such that

$$\mathbf{1}_{\left|\left\langle w_i^{(t)}, x_p\right\rangle\right| \geq b_i^{(t)}} \cdot \mathbf{1}_{\left|\left\langle v_i^{(t)}, y_p\right\rangle\right| \geq b_i^{(t)}} = 0, \tag{91}$$

Using Eq (31), the weight dynamics for $|\langle w_i^{(t+1)}, \mathbf{M}_j\rangle|$ can be expressed as when $T_1 < t \leq T_2$:

$$|\langle w_i^{(t+1)}, \mathbf{M}_j\rangle| \leq \left(1+o\left(\frac{\eta}{d^2}\right)\right)^t \left(\frac{\langle w_i^{(T_1)}, \mathbf{M}_j\rangle + \langle v_i^{(T_1)}, \mathbf{H}_{j'}\rangle + \langle w_i^{(T_1)}, \mathbf{M}_{\mathbf{j'}}\rangle + \langle v_i^{(T_1)}, \mathbf{H}_j\rangle}{4}\right) \tag{92}$$

Because $\left(1+o\left(\frac{\eta}{d^2}\right)\right)^{T_2} \leq 1+o\left(\frac{1}{d}\right)$, the growth in $|\langle w_i^{(T_2)}, \mathbf{M}_j\rangle|$ is negligible. Consequently, we have:

$$|\langle w_i^{(T_2)}, \mathbf{M}_j\rangle|^2 \leq \left(1+o\left(\frac{1}{d}\right)\right) |\langle w_i^{(T_1)}, \mathbf{M}_j\rangle|^2. \tag{93}$$

### E.3. Summary

When $T_2 = \Theta\left(\frac{d\log d}{\eta}\right)$, we know $\left(1+\eta\frac{C_z}{d}\right)^{T_2} = poly(d)$. Using Eq (76), we can ensure that when all neurons satisfy the following condition:

$$\|w_i^{(T_2)}\|_2 \geq \Omega(d)\|w_i^{(T_1)}\|_2, \tag{94}$$

we terminate the training process at $T_2 = \Theta\left(\frac{d\log d}{\eta}\right)$. This ensures that the alignment has sufficiently progressed for effective learning.

Thus, using Eq (93) and Eq (71) we have

$$\begin{aligned}
|\langle w_i^{(T_2)}, \mathbf{M}_j\rangle|^2 + |\langle w_i^{(T_2)}, \mathbf{M}_{j'}\rangle|^2 &= \|w_i^{(T_2)}\|_2^2 - \sum_{j\in[d], j\notin\mathcal{N}_i} \langle w_i^{(T_2)}, \mathbf{M}_j\rangle^2 - \sum_{j\in[d_1]\setminus[d]} \langle w_i^{(T_2)}, \mathbf{M}_j^{\perp}\rangle^2 \\
&\geq \|w_i^{(T_2)}\|_2^2 - (1+o(\frac{1}{d}))(\|w_i^{(T_1)}\|_2^2 - |\langle w_i^{(T_1)}, \mathbf{M}_j\rangle|^2 - |\langle w_i^{(T_1)}, \mathbf{M}_{j'}\rangle|^2) \\
&\geq \|w_i^{(T_2)}\|_2^2 - \|w_i^{(T_1)}\|_2^2 - o(\frac{\|w_i^{(T_1)}\|_2^2}{d})
\end{aligned} \tag{95}$$

Thus, at this stage ($T_1 < t \leq T_2$), we do not consider the worst-case scenario where the probability bounds for feature coupling satisfy

$$\frac{\log(1/c_0)}{2\log d} < \Pr(|z_{y_p}^{j'}| = 1 \mid |z_{x_p}^j| = 1) < \frac{1}{2} < \Pr(|z_{y_p}^j| = 1 \mid |z_{x_p}^j| = 1) < 1$$

We summarize the results when $T_1 < t \leq T_2$ as follows:

1. For $i \in S_{j,\text{sure}}$, the alignment strength satisfies:

$$|\langle w_i^{(T_2)}, \mathbf{M}_j \rangle|^2 > |\langle w_i^{(T_2)}, \mathbf{M}_{j'} \rangle|^2 \geq \frac{1}{4} \frac{\|w_i^{(T_2)}\|_2^2 + \|v_i^{(T_2)}\|_2^2}{2} \tag{96}$$

where $j'$ represents the corresponding spurious alignment feature.

2. For $i \notin S_{j,\text{pot}}$, the alignment strength satisfies:

$$|\langle w_i^{(T_1)}, \mathbf{M}_j \rangle|^2 \leq O(\frac{1}{d}) \cdot \frac{\|w_i^{(T_2)}\|_2^2 + \|v_i^{(T_2)}\|_2^2}{2} \tag{97}$$

3. For $\mathbf{M}_j^{\perp}$ where $j \in [d_1] \setminus [d]$, we have:

$$|\langle w_i^{(t+1)}, \mathbf{M}_j^{\perp} \rangle|^2 < O\left(\frac{1}{d_1}\right) \cdot \frac{\|w_i^{(T_2)}\|_2^2 + \|v_i^{(T_2)}\|_2^2}{2}. \tag{98}$$

These results demonstrate that when $T_1 < t \leq T_2$, the alignment for $i \in S_{j,\text{sure}}$, including the corresponding spurious alignment, grows significantly larger. In contrast, the alignment strength for $i \notin S_{j,\text{pot}}$ and noisy features $\mathbf{M}^{\perp}$ remains unchanged. Similar results also hold for $v_i$.

## Appendix F. ITCP on Raw Data III Convergence

In the previous section, we demonstrated that for $t \leq T_2$, the neurons $(w_i, v_i)$ are sparsely activated and remain consistently activated for $i \in S_{j,\text{sure}}$. Building on this result, this section establishes the convergence of these neurons to sparse solutions, providing a detailed analysis of their behavior during Phase III of ITCP on Raw Data. The following theorem outlines the convergence guarantees under these conditions.

The Phase III of ITCP on Raw Data is defined as the training iterations $T_2 < t \leq T_3$, where $T_3 - T_2 = \Theta(d)$. At the beginning of this phase, we fix the bias threshold as $b_i^{(t)} = b_i^{T_2}$ for $T_2 < t \leq T_3$. Because $b_i^{(T_2)} = \left(1 + \frac{\eta}{d}\right)^{\Theta(d \log d/\eta)} b_i^{(T_1)}$, it is easy to know that for $t \geq T_2$, only when $(x_p, y_p)$ and $(x_n, y_n)$ contain the true feature $j$ and its corresponding spurious feature $j'$, the indicator functions remain consistently activated for $i \in S_{j,\text{sure}}$.

Consequently, using Eq (24), Eq (27), and Eq (28), the loss function $L$ becomes convex with respect to $w_i$ and $v_i$ independently when $(x_p, y_p)$ and $(x_n, y_n)$ contain the true feature $j$ and its corresponding spurious feature $j'$ .

At the end of Phase II, using Eq (81), we know that $\|w_i^{(T_2)}\|_2 \geq \Omega(d)$. Consequently, we cannot only consider $-\langle f^{(t)}(x_p), h^{(t)}(y_p) \rangle$, and the error term $Err_t$ becomes non-negligible.

Specifically, based on Eq (24), it can be observed that the term $-\langle f^{(t)}(x_p), h^{(t)}(y_p) \rangle$ is convex and $l_{i,j,1} = \|x_p\|_2 \|y_p\|_2 = \Theta(1)$-smooth. This ensures that the true features contribute consistently to the optimization process.

Additionally, $L_{i,j,2} = \frac{\left(\langle f^{(t)}(x_n), h^{(t)}(y_p) \rangle\right)^2}{2\tau}$ is also convex, and we further establish its smoothness to provide a rigorous understanding of its behavior.

To analyze the $l_{i,j,2}$-smoothness, we aim to find an upper bound that satisfies:

$$\|\nabla_{w_i, v_i} L_2(w_{i,1}, v_{i,1}) - \nabla_{w_i, v_i} L_2(w_{i,2}, v_{i,2})\|_2 \leq l_{i,j,2} \|(w_{i,1} - w_{i,2}, v_{i,1} - v_{i,2})\|_2. \tag{99}$$

The gradient difference for $w_i$ is given by:

$$\begin{aligned}\|\nabla_{w_i} L_{i,j,2}(w_{i,1}, v_{i,1}) - \nabla_{w_i} L_{i,j,2}(w_{i,2}, v_{i,2})\|_2 &= \frac{\left\| \left(x^\top W_1^\top V_1 y\right) x (v_{i,1} y)^\top - \left(x^\top W_2^\top V_2 y\right) x (v_{i,2} y)^\top \right\|_2}{2\tau} \\ &\leq \frac{l_{w_i,1}}{2\tau} \|w_{i,1} - w_{i,2}\|_2 + \frac{l_{w_i,2}}{2\tau} \|v_{i,1} - v_{i,2}\|_2,\end{aligned} \tag{100}$$

where $l_{w_i,1} = \|x_n\|_2^2 \|y_p\|_2^2 \|v_{i,1}\|_2 \|v_{i,2}\|_2 \leq O(d)$ and $l_{w_i,2} = \|x_n\|_2^2 \|y_p\|_2^2 \big(\|v_{i,1}\|_2 \|w_{i,2}\|_2 + \|w_{i,1}\|_2 \|v_{i,1}\|_2\big) \leq O(d)$.

Similarly, the gradient difference for $v_i$ is:

$$\|\nabla_{v_i} L_{i,j,2}(w_{i,1}, v_{i,1}) - \nabla_{v_i} L_{i,j,2}(w_{i,2}, v_{i,2})\|_2 \leq \frac{l_{v_i,1}}{2\tau} \|w_{i,1} - w_{i,2}\|_2 + \frac{l_{v_i,2}}{2\tau} \|v_{i,1} - v_{i,2}\|_2, \tag{101}$$

where $l_{v_i,1} \leq O(d)$ and $l_{v_i,2} \leq O(d)$.

Combining the results, we find:

$$l_{i,j,2} = \frac{\sqrt{l_{w_i,1}^2 + l_{w_i,2}^2 + l_{v_i,1}^2 + l_{v_i,2}^2}}{2\tau} \leq O(1). \tag{102}$$

Thus, the total smoothness constant is:

$$l_{i,j} = l_{i,j,1} + l_{i,j,2} = \Theta(1). \tag{103}$$

These results demonstrate that the loss function $L$ remains convex and $l_{i,j}$-smooth for neurons $(w_i, v_i)$ when $(x_p, y_p)$ and $(x_n, y_n)$ contain the true feature $j$ and its corresponding spurious feature $j'$ during Phase III of ITCP on Raw Data, ensuring their convergence to sparse solutions while maintaining consistency in their activation patterns.

We verify that the following inequality holds

$$\begin{aligned}L_j(w_i^{(t+1)}, v_i^{(t+1)}) \leq L_j(w_i^{(t)}, v_i^{(t)}) \\ &+ \left\langle \nabla L_j(w_i^{(t)}, v_i^{(t)}), \left(w_i^{(t+1)} - w_i^{(t)},\ v_i^{(t+1)} - v_i^{(t)}\right) \right\rangle \\ &+ \frac{l_{i,j}}{2} \left\| \left(w_i^{(t+1)} - w_i^{(t)},\ v_i^{(t+1)} - v_i^{(t)}\right) \right\|^2\end{aligned} \tag{104}$$

Let $L = \max_{i \in m}(l_{i,j}/(2\tau)) = \Theta(1)$ and $\eta = \frac{1}{L}$ to ensure a monotonic decrease, plug Eq (25) and Eq (26) into Eq (178), we have

$$L_j(w_i^{(t+1)}, v_i^{(t+1)}) \leq L_j(w_i^{(t)}, v_i^{(t)}) - \frac{\eta}{2} \|\nabla L_j(w_i^{(t)}, v_i^{(t)})\|^2. \tag{105}$$

Under our data assumptions for $S_w$ and conclusion in Eq (96) , we define $w_i^* = \alpha_{i,j}^* \mathbf{M}_j + \alpha_{i,j'}^* \mathbf{M}_{j'}, v_i^* = \alpha_{i,j}^* \mathbf{H}_j + \alpha_{i,j'}^* \mathbf{H}_{j'}$. Thus, $L_j(w_i^*, v_i^*)$ captures both the alignment with the true feature $\mathbf{M}_j, \mathbf{H}_j$ and the spurious feature $\mathbf{M}_{j'}, \mathbf{H}_{j'}$, representing the minimal loss achievable under the influence of both true and spurious features in the optimization process. Using Eq (81), we know $w_i^{(T_2)} = \Theta(d)$, so $L_j(w_i^*, v_i^*) = -\Theta(d)$.

By the property of smoothness, we have

$$\|\nabla L_j(w_i^{(t)}, v_i^{(t)})\|_2^2 \geq \frac{2}{L} \left(L_j(w_i^{(t)}, v_i^{(t)}) - L_j(w_i^*, v_i^*)\right) \tag{106}$$

Take the telescope sum of from $T_2$ to $T_3$, we have

$$\begin{aligned}\frac{1}{T_3-T_2}\sum_{t=T_2}^{T_3} L_j(w_i^{(t)}, v_i^{(t)}) &\leq L_j(w_i^*, v_i^*) + \frac{L^2\Delta_0}{T_3-T_2} \\ &\overset{\diamondsuit}{\leq} L_j(w_i^*, v_i^*) + \Theta(1)\end{aligned} \tag{107}$$

where $\Delta_0 = L_j(w_i^{(T_1)}, v_i^{(T_1)}) - L_j(w_i^*, v_i^*) = \Theta(d)$. In $\diamondsuit$, we use $T_3 - T_2 = \Theta(d)$, and $L = \Theta(1)$ .

Generalized to every $j \in d$, the same convergence holds for all $i \in S_{j,\text{sure}}$ when $(x_p, y_p)$ and $(x_n, y_n)$ contain feature $j, j'$. For all $(x_p, y_p)$ and $(x_n, y_n)$ in $S_w$, the following inequality holds:

$$\frac{1}{T_3-T_2}\sum_{t=T_2}^{T_3} L(f^{(T_3)}, h^{(T_3)}) \leq L(f^*, h^*) + \Theta(1). \tag{108}$$

As a result, the relative difference is bounded by:

$$\frac{L(f^{(T_3)}, h^{(T_3)}) - L(f^*, h^*)}{|L(f^*, h^*)|} \leq \Theta\left(\frac{1}{d}\right). \tag{109}$$

### F.1. Summary

ITCP trained on raw data $S$ undergoes Stages D–F. After $T = \Theta(d^2 \log d)$ SGD iterations with batch size $B = \Omega(d)$ and learning rate $\eta = O(1)$, the resulting weights $(\overline{\mathbf{W}}, \overline{\mathbf{V}})$ minimize the contrastive loss in Eq. (1) up to a vanishing relative error:

$$\frac{L(f_{\overline{\mathbf{W}}}, h_{\overline{\mathbf{V}}}) - L^*}{|L^*|} \leq o(1). \tag{110}$$

However, each neuron pair $(\bar{w}_i, \bar{v}_i)$ in $(\overline{\mathbf{W}}, \overline{\mathbf{V}})$, for $i \in [m]$, predominantly encodes a mixture of features indexed by a subset $N_i \subseteq [d]$, with $|N_i| \geq 2$. Specifically, we have:

$$\begin{aligned}\bar{w}_i &= \sum_{j\in N_i} \alpha_{i,j}\mathbf{M}_j + \sum_{j\in[d]\setminus N_i} \beta_{i,j}\mathbf{M}_j + \sum_{j\in[d_1]\setminus[d]} \gamma_{i,j}\mathbf{M}_j^{\perp}, \\ \bar{v}_i &= \sum_{j\in N_i} \alpha_{i,j}\mathbf{H}_j + \sum_{j\in[d]\setminus N_i} \beta_{i,j}\mathbf{H}_j + \sum_{j\in[d_1]\setminus[d]} \gamma_{i,j}\mathbf{H}_j^{\perp},\end{aligned} \tag{111}$$

where $\alpha_{i,j}^2 = \Theta(\|\bar{w}_i\|_2^2 + \|\bar{v}_i\|_2^2)$, and the interference from other features is small: $\beta_{i,j}/\alpha_{i,j} \leq O(1/\sqrt{d})$, $\gamma_{i,j}/\alpha_{i,j} \leq O(1/\sqrt{d_1})$.

Moreover, for every spuriously correlated feature pair $(j, j')$ satisfying Assumption 3, there exists at least an $\Omega(1)$ many of neurons $i \in [m]$ with $N_i = \{j, j'\}$, indicating the prevalence of feature mixing due to data misalignment.

## Appendix G. Captioning

In this stage, the model fine-tunes the pre-trained encoder parameters $\mathbf{W}$ and $\mathbf{V}$ to obtain the updated parameters $\hat{\mathbf{W}}$ and $\hat{\mathbf{V}}$ through Image-Text Contrastive Pre-training (ITCP) on raw data.

Given an image-text pair $(x_p, y_p)$ in $S_w$, the decoder generates synthetic captions $\hat{y}_p = \hat{\mathbf{V}}^T \sigma(\hat{\mathbf{W}} x_p)$, where $\sigma(\cdot)$ denotes the activation function. The Image-Grounded Text Decoder, initialized with $\mathbf{W}$ and $\mathbf{V}$ from the pre-trained encoders, is fine-tuned on $S_h$ by minimizing the following loss function:

$$L_C = \mathbb{E}_{(x_p, y_p) \in S_h} \left[ \frac{1}{2} \left\| \mathbf{V}^T \sigma(\mathbf{W} x_p) - y_p \right\|_2^2 \right], \tag{112}$$

where $\|\cdot\|_2$ denotes the Euclidean norm. This fine-tuning process refines the model to generate captions that are more closely aligned with the target text data in $S_h$.

During the captioning, we sample a batch of image-text pairs $S_h^{(t)} = \{(x_p, y_p)\}_{p=1}^B \subseteq S_h$. We perform stochastic gradient descent on $L_C$. At each iteration, we update as

$$w_i^{(t+1)} \leftarrow w_i^{(t)} - \eta \nabla_{w_i} L_C^{(t)} \tag{113}$$

$$v_i^{(t+1)} \leftarrow v_i^{(t)} - \eta \nabla_{v_i} L_C^{(t)} \tag{114}$$

At the beginning of this phase, we set the bias threshold as:

$$b_i^{(0)} = \sqrt{\frac{\|w_i^{(T_2)}\|_2^2 - \|w_i^{(T_1)}\|_2^2}{2}} \tag{115}$$

During training, the bias threshold is iteratively updated as:

$$b_i^{(t+1)} = \left(1 + \frac{\eta}{d}\right) b_i^{(t)}, \tag{116}$$

The gradient of $L_C$ with respect to $w_i^{(t)}$, $v_i^{(t)}$, $\mathbf{W}$, and $\mathbf{V}$ at iteration $t$ is given by:

$$\nabla_{w_i^{(t)}} L_C = v_i^{(t)} (y_p - \mathbf{V}^T \mathbf{W} x_p) x_p^T \cdot \mathbf{1}_{\left|\left\langle w_i^{(t)}, x_p \right\rangle\right| \geq b_i^{(t)}} \tag{117}$$

$$\nabla_{v_i^{(t)}} L_C = w_i^{(t)} x_p (y_p - \mathbf{V}^T \mathbf{W} x_p)^T \cdot \mathbf{1}_{\left|\left\langle w_i^{(t)}, x_p \right\rangle\right| \geq b_i^{(t)}} \tag{118}$$

The alignment can be described by the following update rule:

$$\begin{aligned} \langle w_i^{(t+1)}, \mathbf{M}_j \rangle &= \langle w_i^{(t)}, \mathbf{M}_j \rangle - \langle \nabla_{w_i} L_C, \mathbf{M}_j \rangle \\ &= \langle w_i^{(t)}, \mathbf{M}_j \rangle + \eta \cdot \mathrm{tr}(v_i^{(t)\top} (y_p - \mathbf{V}^T \mathbf{W} x_p) x_p^T \mathbf{M}_j \cdot \mathbf{1}_{|\langle w_i, x_p \rangle| \geq b_i^{(t)}}) \end{aligned} \tag{119}$$

$$\begin{aligned} \langle v_i^{(t+1)}, \mathbf{H}_j \rangle &= \langle v_i^{(t)}, \mathbf{H}_j \rangle - \langle \nabla_{v_i} L_C, \mathbf{H}_j \rangle \\ &= \langle v_i^{(t)}, \mathbf{H}_j \rangle + \eta \cdot \mathrm{tr}(w_i^{(t)\top} x_p (y_p - \mathbf{V}^T \mathbf{W} x_p)^T \mathbf{H}_j \cdot \mathbf{1}_{\left|\left\langle w_i^{(t)}, x_p \right\rangle\right| \geq b_i^{(t)}}) \end{aligned} \tag{120}$$

### G.1. Alignment for $i \in S_{j,\text{sure}}$

This section analyzes the alignment growth for neurons $i \in S_{j,\text{sure}}$. Specifically, we show that when $t \leq T_C$, the alignment with the true feature $\mathbf{M}_j$ grows exponentially if $x_p$ contains the true feature $\mathbf{M}_j$. In contrast, the alignment with the spurious feature $\mathbf{M}_{j'}$ exhibits negligible growth, even for neurons $i \in S_{j,\text{sure}}$. Specially,

1. For the true feature $\mathbf{M}_j$, based on the result in Eq (96) and the bias threshold in Eq (115), the indicator functions are always activated. This ensures that the neuron can consistently increase its alignment in the direction of the true feature $\mathbf{M}_j$.

2. For the spurious feature $\mathbf{M}_{j'}$, based on the result in Eq (96) and the bias threshold in Eq (115), the indicator functions remain non-activated. This prevents the neuron from increasing its alignment in the direction of the spurious feature $\mathbf{M}_{j'}$.

The details of proof as follow:

Using Eq (95), we know

$$\|w_i^{(T_2)}\|_2^2 - \|w_i^{(T_1)}\|_2^2 \geq |\langle w_i^{(T_2)}, \mathbf{M}_j\rangle|^2 + |\langle w_i^{(T_2)}, \mathbf{M}_{j'}\rangle|^2 \geq \|w_i^{(T_2)}\|_2^2 - \|w_i^{(T_1)}\|_2^2 - o(\frac{\|w_i^{(T_1)}\|_2^2}{d}) \tag{121}$$

Using Eq (32) and Eq (33), we have

$$\langle w_i^{(t)}, \mathbf{M}_j\rangle - \langle w_i^{(t)}, \mathbf{M}_{j'}\rangle = \frac{(a+b-c)^t}{2}\left(\langle w_i^{(0)}, \mathbf{M}_j\rangle + \langle v_i^{(0)}, \mathbf{H}_j\rangle - \langle w_i^{(0)}, \mathbf{M}_{j'}\rangle - \langle v_i^{(0)}, \mathbf{H}_{j'}\rangle\right) + Err_t \tag{122}$$

Using Eq (40) and $(a+b-c)^{T_1+T_2} \geq \Omega(d^2)$, with high probability $1 - O(\frac{1}{\sqrt{d}})$ we have,

$$|\langle w_i^{(T_2)}, \mathbf{M}_j\rangle|^2 - |\langle w_i^{(T_2)}, \mathbf{M}_{j'}\rangle|^2 \geq \Omega(\frac{\|w_i^{(T_1)}\|_2^2}{d}) \tag{123}$$

Therefore, with high probability $1 - O(\frac{1}{\sqrt{d}})$ we have

$$|\langle w_i^{(T_2)}, \mathbf{M}_j\rangle|^2 > \frac{\|w_i^{(T_2)}\|_2^2 - \|w_i^{(T_1)}\|_2^2}{2} > |\langle w_i^{(T_2)}, \mathbf{M}_{j'}\rangle|^2 \tag{124}$$

We set $b_i^{(0)} = \sqrt{\frac{\|w_i^{(T_2)}\|_2^2 - \|w_i^{(T_1)}\|_2^2}{2}}$, and using Eq (124), so similarly to the proof of Eq (86) we can prove:

1. For $i \in S_{j,\text{sure}}$ and $x_p$ contain the true feature $\mathbf{M}_j$, with high probability $1 - O(\frac{1}{\sqrt{d}})$ the indicator functions become consistently activated $0 \leq t \leq T_C$ such that:

$$\mathbf{1}_{\left|\left\langle w_i^{(t)}, x_p\right\rangle\right| \geq b_i^{(t)}} = 1 \tag{125}$$

2. For $i \in S_{j,\text{sure}}$ and $x_p$ contain the corresponding spurious aligned feature $\mathbf{M}_{j'}$, with high probability $1 - O(\frac{1}{\sqrt{d}})$ the indicator functions become consistently activated $0 \leq t \leq T_C$ such that:

$$\mathbf{1}_{\left|\left\langle w_i^{(t)}, x_p\right\rangle\right| \geq b_i^{(t)}} = 0 \tag{126}$$

3. For $i \notin S_{j,\text{pot}}$ and $\mathbf{M}_j^{\perp}$ where $j \in [d_1] \setminus [d]$, we have:

$$\mathbf{1}_{\left|\left\langle w_i^{(t)}, x_p\right\rangle\right| \geq b_i^{(t)}} = 0 \tag{127}$$

For the residual loss in Eq (119) and Eq (120), we bound the difference if $\mathbf{1}_{\left|\left\langle w_i^{(t)}, x_p\right\rangle\right| \geq b_i^{(t)}} = 1$:

$$\begin{aligned}\mathbf{H}_j z_{x_p}^j z_{y_p}^j &\overset{\diamondsuit}{\geq} (y_p - \mathbf{V}^T \mathbf{W} x_p) x_p^T \mathbf{M}_j \cdot \mathbf{1}_{|\langle w_i, x_p\rangle| \geq b_i^{(t)}} \\ &= (\mathbf{H}_j z_{x_p}^j z_{y_p}^j - \sum_{i=1}^{m} \langle v_i, \mathbf{H}_j\rangle \langle w_i, \mathbf{M}_j\rangle \mathbf{H}_j z_{x_p}^j z_{y_p}^j) \cdot \mathbf{1}_{\langle w_i, x_p\rangle \geq b} \\ &\overset{\heartsuit}{\geq} \mathbf{H}_j z_{x_p}^j z_{y_p}^j - O(d^{\gamma c_0}) \langle v_i, \mathbf{H}_j\rangle \langle w_i, \mathbf{M}_j\rangle \mathbf{H}_j z_{x_p}^j z_{y_p}^j\end{aligned} \tag{128}$$

In $\diamondsuit$, we employ the approximation $y_p x_p^\top \mathbf{M}_j \approx \mathbf{H}_j z_{x_p}^j z_{y_p}^j$, based on the observation that $z_{x_p}^j z_{y_p}^{j'} \ll z_{x_p}^j z_{y_p}^j$ when $j \neq j'$. In $\heartsuit$, we utilize Eq (38). There are at most $O(d^{\gamma c_0})$ neurons capable of learning $\mathbf{M}_j$, which satisfy the condition $\mathbf{1}_{\langle w_i, x_p\rangle \geq b}$.

For $i \in S_{j,\text{sure}}$ and for $x_p$ contain $\mathbf{M}_j$, using Eq (128), Eq (119) and Eq (126) we have:

$$\begin{aligned}\langle w_i^{(t+1)}, \mathbf{M}_j\rangle &\geq \langle w_i^{(t)}, \mathbf{M}_j\rangle + \eta \cdot \operatorname{tr}\left(v_i^{(t)} \cdot (1-\alpha_t^2) \mathbf{H}_j \mathbb{E}\left[z_{x_p}^j z_{y_p}^j\right]\right) \\ &\geq \langle w_i^{(t)}, \mathbf{M}_j\rangle + \eta \frac{C_z(1-\alpha_t^2)}{d} \langle v_i^{(t)}, \mathbf{H}_j\rangle,\end{aligned} \tag{129}$$

Similar to Eq (32), we have

$$|\langle w_i^{(t)}, \mathbf{M}_j\rangle| \geq \left(1 + \eta \frac{C_z \cdot (1-\alpha_t^2)}{d}\right)^t \left(\frac{\langle w_i^{(0)}, \mathbf{M}_j\rangle + \langle v_i^{(0)}, \mathbf{H}_j\rangle}{2}\right) \tag{130}$$

Similarly, for $i \in S_{j,\text{sure}}$ and $x_p$ contain the corresponding spurious aligned feature $\mathbf{M}_{j'}$, because $\Pr[\mathbf{1}_{\left|\left\langle w_i^{(t)}, x_p\right\rangle\right| \geq b_i^{(t)}} = 0] \geq 1 - O(\frac{1}{\sqrt{d}})$, we have

$$\langle w_i^{(t+1)}, \mathbf{M}_{j'}\rangle \leq \langle w_i^{(t)}, \mathbf{M}_{j'}\rangle + O(\frac{\eta}{d^{1.5}}) \langle v_i^{(t)}, \mathbf{H}_{j'}\rangle \tag{131}$$

and

$$|\langle w_i^{(t)}, \mathbf{M}_{j'}\rangle| \leq \left(1 + O(\frac{\eta}{d^{1.5}})\right)^t \left(\frac{\langle w_i^{(T_2)}, \mathbf{M}_{j'}\rangle + \langle v_i^{(T_2)}, \mathbf{H}_{j'}\rangle}{2}\right) \tag{132}$$

At $T_C = \Theta\left(\frac{d \log(d)}{\eta}\right)$, we have:

$$\frac{|\langle w_i^{(T_C)}, \mathbf{M}_j\rangle|}{|\langle w_i^{(T_C)}, \mathbf{M}_{j'}\rangle|} > \frac{\left(1 + \eta \frac{C_z \cdot (1-\alpha_t^2)}{d}\right)^{T_C}}{\left(1 + O(\frac{\eta}{d^{1.5}})\right)^{T_C}} \geq \Omega(d) \tag{133}$$

Therefore, we summarize that when $t = T_C$, the alignment with the true feature $\mathbf{M}_j$ dominates, satisfying:

$$\frac{|\langle w_i^{(T_C)}, \mathbf{M}_j\rangle|}{|\langle w_i^{(T_C)}, \mathbf{M}_{j'}\rangle|} \geq \Omega(d), \tag{134}$$

highlighting the significant separation between the true feature $\mathbf{M}_j$ and the spurious feature $\mathbf{M}_{j'}$ for neurons $i \in S_{j,\text{sure}}$. A similar result holds for $v_i$, where the alignment with the true feature $\mathbf{H}_j$ similarly dominates over the spurious feature $\mathbf{H}_{j'}$.

## G.2. Convergence

For $i \in S_{j,\text{sure}}$, when $x_p, y_p$ contains the true feature $j$, the indicator functions remain consistently activated. Consequently, the loss function $L_C$ becomes convex with respect to $w_i$ and $v_i$ independently. We verify that the following inequality holds

$$\begin{aligned} L_{C,j}(w_i^{(t+1)}, v_i^{(t+1)}) \leq L_{C,j}(w_i^{(t)}, v_i^{(t)}) \\ + \left\langle \nabla L_{C,j}(w_i^{(t)}, v_i^{(t)}), (w_i^{(t+1)} - w_i^{(t)}, v_i^{(t+1)} - v_i^{(t)}) \right\rangle \\ + \frac{l_i}{2} \left\| (w_i^{(t+1)} - w_i^{(t)}, v_i^{(t+1)} - v_i^{(t)}) \right\|^2 \end{aligned} \tag{135}$$

where $l_i = O(C_z d^{2\gamma c_0})(\left\| v_i^{(t)} \right\|_2^2 \|x_p\|_2^2 + \left\| v_i^{(t)} \right\|_2^2 \|x_p\|_2^2) = \Theta(1)$. This means $L_{C,j}(w_i^{(t)}, v_i^{(t)})$ is $l_i$-smooth for all $i \in S_{j,\text{sure}}$ when $x_p, y_p$ contains the true feature $j$. Let $L = \max_{i \in m}(l_i) = \Theta(1)$

Let $\eta = \frac{1}{L}$ to ensure a monotonic decrease, plug Eq (117) and Eq (118) into Eq (135), we have

$$L_{C,j}(w_i^{(t+1)}, v_i^{(t+1)}) \leq L_{C,j}(w_i^{(t)}, v_i^{(t)}) - \frac{\eta}{2} \|\nabla L_{C,j}(w_i^{(t)}, v_i^{(t)})\|^2. \tag{136}$$

By the property of smoothness, we have

$$\|\nabla L_{C,j}(w_i^{(t)}, v_i^{(t)})\|_2^2 \geq \frac{2}{L} \left( L_{C,j}(w_i^{(t)}, v_i^{(t)}) - L_{C,j}(w_i^*, v_i^*) \right). \tag{137}$$

Take the telescope sum of from 0 to $T_C$, we have

$$\begin{aligned} \frac{1}{T_C} \sum_{t=0}^{T_C} L_{C,j}(w_i^{(t)}, v_i^{(t)}) &\leq L_{C,j}(w_i^*, v_i^*) + \frac{L^2 \Delta_0}{T_C} \\ &\overset{\diamondsuit}{\leq} L_{C,j}(w_i^*, v_i^*) + \Theta(\frac{1}{d}) \\ &\overset{\heartsuit}{=} \Theta(\frac{1}{d}) \end{aligned} \tag{138}$$

where $\Delta_0 = L_{C,j}(w_i^{(0)}, v_i^{(0)}) - L_{C,j}(w_i^*, v_i^*)$. In $\diamondsuit$, we use $T_C = \Theta(d)$, and $\|w_i^{(t)}\|_2^2 = \|v_i^{(t)}\|_2^2 = \Theta(1)$. In $\heartsuit$, we use $w_i^* = \alpha_{i,j}^* \mathbf{M}_j, V_i^* = \alpha_{i,j}^* \mathbf{H}_j$ and $L_{C,j}(w_i^*, v_i^*) = \Theta(\frac{1}{d})$ if $x_p$ contains the true feature $\mathbf{M}_j$.

Therefore, for all $j \in d$ and all $(x_p, y_p) \in S_h$, when $T_C = \Theta(d^2)$, we can ensure

$$L_C = \mathbb{E}_{(x_p, y_p) \in S_h} \left[ \frac{1}{2} \left\| \mathbf{V}^T \sigma(\mathbf{W} x_p) - y_p \right\|_2^2 \right] \leq \Theta(\frac{1}{d}) \tag{139}$$

## G.3. Summary

After $T_C$ iterations, the parameters $\mathbf{W}$ and $\mathbf{V}$ are updated to $\mathbf{W}^{T_C} = \hat{\mathbf{W}}$ and $\mathbf{V}^{T_C} = \hat{\mathbf{V}}$, respectively, using the dataset $S_h$. The generated caption is given by:

$$\hat{y}_p = \hat{\mathbf{V}}^T \sigma(\hat{\mathbf{W}} x_p), \tag{140}$$

where the expected loss satisfies:

$$\mathbb{E}\left[\frac{1}{2}\left\|\hat{y}_p - y_p\right\|_2^2\right] = L_C \leq \Theta\left(\frac{1}{d}\right). \tag{141}$$

1. For $i \in S_{j,\text{sure}}$, the alignment strength satisfies:

$$|\langle w_i^{(T_C)}, \mathbf{M}_j \rangle|^2 = \Theta(1) \left\|w_i^{(T_C)}\right\|_2^2 \tag{142}$$

and

$$|\langle w_i^{(T_C)}, \mathbf{M}_j' \rangle|^2 \leq O(\frac{1}{d}) \left\|w_i^{(T_C)}\right\|_2^2 \tag{143}$$

where $j'$ represents the corresponding spurious alignment feature.

2. For $i \notin S_{j,\text{pot}}$, the alignment strength satisfies:

$$|\langle w_i^{(T_1)}, \mathbf{M}_j \rangle|^2 \leq O(\frac{1}{d}) \left\|w_i^{(T_C)}\right\|_2^2 \tag{144}$$

3. For $\mathbf{M}_j^{\perp}$ where $j \in [d_1] \setminus [d]$, we have:

$$|\langle w_i^{(t+1)}, \mathbf{M}_j^{\perp} \rangle|^2 < O(\frac{1}{d_1}) \left\|w_i^{(T_C)}\right\|_2^2 \tag{145}$$

## Appendix H. Filtering

During filtering, we sample the synthetic image-text pair $(x_p, \hat{y}_p)$ in $\hat{S}_w$ and the corresponding image-text pair $(x_p, y_p)$ in $S_w$. The image encoder $f$ and text encoder $h$ trained on raw data are employed to obtain the corresponding embeddings.

$$z'_{x_p} = f(x_p), \quad \hat{z}_{y_p} = h(\hat{y}_p), \quad z'_{y_p} = h(y_p) \tag{146}$$

Then, we calculate the cosine similarity of $\langle z'_{x_p}, \hat{z}_{y_p} \rangle$ and $\langle z'_{x_p}, z'_{y_p} \rangle$, and select the image-text pair with higher cosine similarity denoted as $(x, \tilde{y})$. In this way, we replace the noisy pairs in $S_w$ with synthetic pairs in $\hat{S_w}$. The resulting dataset is denoted as $\tilde{S} = \tilde{S}_w \cup S_h$.

The decoder generates synthetic captions $\hat{y}_p = \hat{\mathbf{V}}^T \sigma(\hat{\mathbf{W}} x_p)$. Using Eq (141), for each data pair $(x_p, y_p)$ which contain feature $(\mathbf{M}_j, \mathbf{H}_j)$ in $S_h$ we have

$$\mathbb{E}_{(x_p,y_p)}\left[\mathbb{E}_{j\in d}\left[\frac{1}{2}\left\|\mathbf{H}_j z^j_{\hat{y}_p} - \mathbf{H}_j z^j_{y_p}\right\|_2^2\right] ||z^j_{y_p}| = 1\right] \leq \mathbb{E}_{(x_p,y_p)}\left[\frac{1}{2}\left\|\hat{y}_p - y_p\right\|_2^2 ||z^j_{y_p}| = 1\right] = L_C \leq \Theta(\frac{1}{d}) \tag{147}$$

Therefore, using $\|\mathbf{H}_j\|_2 = 1$ and $z_{x_p} = z_{y_p}$ in $S_h$, we have

$$\mathbb{E}_{x_p, j\in d}\left[z^j_{\hat{y}_p} z^j_{x_p} ||z^j_{x_p}| = 1\right] \geq 1 - \Theta(\frac{1}{d}) \tag{148}$$

Base on Assumption 4 $z^j_{x_p} \sim$ Bernoulli $\left(\frac{C_z}{d}\right)$, we have

$$\Pr(z^j_{\hat{y}_p} = 1 \mid |z^j_{x_p}| = 1) \geq 1 - \Theta(\frac{1}{d}) \tag{149}$$

Using Eq (134) and Eq (149), we have

$$\Pr(z_{\hat{y}_p}^{j'} = 1 \mid |z_{x_p}^j| = 1) \leq \Theta(\frac{1}{d}) \tag{150}$$

Therefore, after replace all noisy text $y_p$ in $S_w$ by synthetic caption $\hat{y}_p$ in $\hat{S_w}$
1. for a positive pair $(x_p, y_p)$, we have

$$\mathbb{E}\left[z_{\tilde{x}_p}^j z_{\tilde{y}_p}^j\right] = \Theta(\frac{1}{d}), \quad \mathbb{E}\left[z_{\tilde{x}_p}^j z_{\tilde{y}_p}^{j'}\right] = \Theta\left(\frac{1}{d^2}\right), \quad \forall j' \neq j. \tag{151}$$

2. for negative pairs $(x_p, y_q)$, where $p \neq q$, we have:

$$\mathbb{E}\left[z_{x_p}^j z_{y_q}^{j'}\right] = \Theta\left(\frac{1}{d^2}\right), \quad \forall j, j' \in [d]. \tag{152}$$

## Appendix I. ITCP on Synthetic (Recaptioned) Data

During ITCP on Raw Data, we use a noisy dataset $S$. Based on SubSection B.2, we have $\mathbb{E}\left[z_x^j z_y^j\right]$ and $\mathbb{E}\left[z_x^j z_y^{j'}\right]$ both in $\Theta\left(\frac{1}{d}\right)$. In this scenario, for $i \in S_{j,\text{sure}}$, $w_i^{(t)}$ is jointly influenced by $\mathbf{M}_j$ and $\mathbf{M}_{j'}$, with both features contributing comparably to the updates. However, during ITCP on recaptioned data, we sample image-text pairs from the dataset $\tilde{S}$. Using Eq. (151), we find that $\mathbb{E}\left[z_{\tilde{x}_p}^j z_{\tilde{y}_p}^{j'}\right] = \Theta\left(\frac{1}{d^2}\right)$. In this case, for $i \in S_{j,\text{sure}}$, $w_i^{(t)}$ is influenced solely by $\mathbf{M}_j$, without interference from spurious features, ensuring purified representations.

The only difference between ITCP on Raw Data and Data lies in the $\mathbb{E}\left[z_{\tilde{x}_p}^j z_{\tilde{y}_p}^{j'}\right]$; all other training processes remain largely the same. Therefore, we simplify our proof accordingly.

### I.1. Phase I of ITCP on Synthetic Data

The Phase I of ITCP on Data is defined as the training iterations $t \leq T_1$, where $T_1 = \Theta\left(\frac{d \log d}{\eta}\right)$ is the iteration when all $\|w_i^{(T_2)}\|_2^2 = 2\|w_i^{(0)}\|_2^2$. Before $T_1$, we set $b_i^{(t)} = 0$. For every neuron $i \in [m]$, the weights $w_i$, $v_i$ will mostly ignore the noise features $\mathbf{M}^\perp$, $\mathbf{H}^\perp$ and learn to emphasize the features $\mathbf{M}$, $\mathbf{H}$.

If $\Pr(|z_{y_p}^j| = 1 \mid |z_{x_p}^{j'}| = 1) < 0.1$, we have $\mathbb{E}\left[z_x^j z_y^j\right] \gg \mathbb{E}\left[z_x^j z_y^{j'}\right]$ and $(a+b+c)^t \approx (a+b-c)^t$. In this case, $w_i^{(t+1)}$ is predominantly influenced by $\mathbf{M}_j$, with minimal contributions from $\mathbf{M}_{j'}$. The updates are thus primarily driven by the single feature $\mathbf{M}_j$, ensuring that spurious interactions from $\mathbf{M}_{j'}$ are negligible.

$$\begin{aligned}\|\mathbf{M}\mathbf{M}^\top w_i^{(t)}\|_2^2 &= \sum_{i=1}^{d}\left[\frac{(a+b+c)^t}{2}\left(\langle w_i^{(t)}, \mathbf{M}_j\rangle + \langle v_i^{(t)}, \mathbf{H}_j\rangle\right)\right]^2 \\ &= \left(1 + \frac{\eta C_z}{d}\right)^{2t} \frac{\|\mathbf{M}\mathbf{M}^\top w_i^{(0)}\|_2^2 + \|\mathbf{H}\mathbf{H}^\top v_i^{(0)}\|_2^2}{4}.\end{aligned} \tag{153}$$

$i \in S_{j,\text{sure}}$:

$$\begin{aligned}
|\langle w_i^{(T_1)}, \mathbf{M}_j \rangle|^2 &= \left(1+\eta\frac{C_z}{d}\right)^{2T_1}\left(\frac{\langle w_i^{(0)}, \mathbf{M}_j\rangle + \langle v_i^{(0)}, \mathbf{H}_j\rangle}{2}\right)^2 \\
&\geq \left(1+\eta\frac{C_z}{d}\right)^{2T_1}\cdot\frac{c_1\log d}{d}\cdot\frac{\|\mathbf{M}\mathbf{M}^\top w_i^{(0)}\|_2^2 + \|\mathbf{H}\mathbf{H}^\top v_i^{(0)}\|_2^2}{4} \\
&= \frac{c_1\log d}{d}\cdot\frac{\|\mathbf{M}\mathbf{M}^\top w_i^{(T_1)}\|_2^2 + \|\mathbf{H}\mathbf{H}^\top v_i^{(T_1)}\|_2^2}{2} \\
&\geq \frac{c_1\log d}{d}\cdot\frac{\|w_i^{(T_1)}\|_2^2 + \|v_i^{(T_1)}\|_2^2 - \|w_i^{(0)}\|_2^2 - \|v_i^{(0)}\|_2^2}{2} \\
&\geq \frac{(1+c_0)\log d}{d}\cdot\frac{\|w_i^{(T_1)}\|_2^2 + \|v_i^{(T_1)}\|_2^2}{2}
\end{aligned} \tag{154}$$

Because $\frac{\|w_i^{(T_1)}\|_2^2 + \|v_i^{(T_1)}\|_2^2}{2} = \|w_i^{(0)}\|_2^2 + \|v_i^{(0)}\|_2^2$ and $c_1 > 2(1+c_0)$

$i \notin S_{j,\text{sure}}$:

$$\begin{aligned}
|\langle w_i^{(T_1)}, \mathbf{M}_j \rangle|^2 &= \left(1+\eta\frac{C_z}{d}\right)^{2T_1}\left(\frac{\langle w_i^{(0)}, \mathbf{M}_j\rangle + \langle v_i^{(0)}, \mathbf{H}_j\rangle}{2}\right)^2 \\
&\leq \left(1+\eta\frac{C_z}{d}\right)^{2T_1}\cdot\frac{c_2\log d}{d}\cdot\frac{\|\mathbf{M}\mathbf{M}^\top w_i^{(0)}\|_2^2 + \|\mathbf{H}\mathbf{H}^\top v_i^{(0)}\|_2^2}{4} \\
&= \frac{c_2\log d}{d}\cdot\frac{\|\mathbf{M}\mathbf{M}^\top w_i^{(T_1)}\|_2^2 + \|\mathbf{H}\mathbf{H}^\top v_i^{(T_1)}\|_2^2}{2} \\
&\leq \frac{\log d}{d}\cdot\frac{\|w_i^{(T_1)}\|_2^2 + \|v_i^{(T_1)}\|_2^2}{2}
\end{aligned} \tag{155}$$

$|\langle w_i^{(t+1)}, \mathbf{M}_\mathbf{j}^\perp\rangle|^2 \leq O(\frac{1}{d_1})\frac{\|w_i^{(T_1)}\|_2^2 + \|v_i^{(T_1)}\|_2^2}{2}$

### I.2. Phase II:

The Phase II of ITCP on Synthetic Data is defined as the training iterations $T_1 \leq t \leq T_2$, where $T_2 - T_1 = \Theta\left(\frac{d\log d}{\eta}\right)$ is the iteration.

We set $b_i^{(t)} = \sqrt{\frac{\log d}{d}\cdot\frac{\|w_i^{(T_1)}\|_2^2 + \|v_i^{(T_1)}\|_2^2}{2}}$ and $b_i^{(t+1)} = (1+\frac{\eta}{d})b_i^{(t)}$ until all $\|\|w_i^{(T_2)}\|_2 \geq \Omega(d)\|w_i^{(T_1)}\|_2$,. In this phase, the weights $(w_i, v_i)$ will mostly ignore the features $\mathbf{M}_j$, $\mathbf{H}_j$ if $i \notin S_{j,\text{sure}}$ and the noise features $\mathbf{M}^\perp$, $\mathbf{H}^\perp$, and learn to emphasize the features $\mathbf{M}_j$, $\mathbf{H}_j$ if $i \in S_{j,\text{sure}}$.

For $i \in S_{j,\text{sure}}$, using Lemma 16, the following holds with high probability $1 - e^{-\Omega(d_1)}$ when $T_1 < t \leq T_2$ :

$$\left|\langle w_i^{(t)}, \xi\rangle\right|^2 \leq O\left(\frac{\left\|w_i^{(t)}\right\|_2^2}{d^{1+c_0}}\right) < b_i^{(t)} \tag{156}$$

Under the assumption that, with high probability, the indicator function satisfies the condition when $t = T_1$:

$$\mathbf{1}_{\left|\left\langle w_i^{(t)}, x_p \right\rangle\right| \geq b_i^{(t)}} \cdot \mathbf{1}_{\left|\left\langle v_i^{(t)}, y_p \right\rangle\right| \geq b_i^{(t)}} = 1, \tag{157}$$

we can ensure that:

$$\mathbb{E}\left[z_x^j z_y^j \cdot \mathbf{1}_{\left|\left\langle w_i^{(t)}, x_p \right\rangle\right| \geq b_i^{(t)}} \cdot \mathbf{1}_{\left|\left\langle v_i^{(t)}, y_p \right\rangle\right| \geq b_i^{(t)}}\right] = \frac{C_z}{d}. \tag{158}$$

The weight dynamics for $|\langle w_i^{(t+1)}, \mathbf{M}_j \rangle|$ can be expressed as:

$$|\langle w_i^{(t+1)}, \mathbf{M}_j \rangle| = \left(1 + \eta \frac{C_z}{d}\right) \left(\frac{\langle w_i^{(t)}, \mathbf{M}_j \rangle + \langle v_i^{(t)}, \mathbf{H}_j \rangle}{2}\right). \tag{159}$$

Given that $\left(1 + \eta \frac{C_z}{d}\right) > \left(1 + \frac{\eta}{d}\right)$, and $\frac{\langle w_i^{(t)}, \mathbf{M}_j \rangle + \langle v_i^{(t)}, \mathbf{H}_j \rangle}{2} > b_i^{(t)}$, it follows that:

$$|\langle w_i^{(t+1)}, \mathbf{M}_j \rangle| > b_i^{(t+1)}. \tag{160}$$

Thus, with high probability, for $t \leq T_2$, we have:

$$\mathbf{1}_{\left|\left\langle w_i^{(t)}, x_p \right\rangle\right| \geq b_i^{(t)}} \cdot \mathbf{1}_{\left|\left\langle v_i^{(t)}, y_p \right\rangle\right| \geq b_i^{(t)}} = 1. \tag{161}$$

so for $T_1 < t \leq T_2$ we have

$$|\langle w_i^{(t+1)}, \mathbf{M}_j \rangle| = \left(1 + \eta \frac{C_z}{d}\right)^t \left(\frac{\langle w_i^{(T_1)}, \mathbf{M}_j \rangle + \langle v_i^{(T_1)}, \mathbf{H}_j \rangle}{2}\right) \tag{162}$$

For $i \notin S_{j,\text{sure}}$, the projection of weights onto a generic feature $\xi$ at iteration $T_1$ satisfies:

$$\Pr\left(\mathbf{1}_{\left|\left\langle w_i^{(t)}, x_p \right\rangle\right| \geq b_i^{(t)}} \cdot \mathbf{1}_{\left|\left\langle v_i^{(t)}, y_p \right\rangle\right| \geq b_i^{(t)}} = 1\right) \leq o\left(\frac{1}{d}\right). \tag{163}$$

We can ensure that:

$$\mathbb{E}\left[z_x^j z_y^j \cdot \mathbf{1}_{\left|\left\langle w_i^{(t)}, x_p \right\rangle\right| \geq b_i^{(t)}} \cdot \mathbf{1}_{\left|\left\langle v_i^{(t)}, y_p \right\rangle\right| \geq b_i^{(t)}}\right] = o\left(\frac{1}{d^2}\right). \tag{164}$$

The weight dynamics for $|\langle w_i^{(t+1)}, \mathbf{M}_j \rangle|$ can now be expressed as:

$$|\langle w_i^{(t+1)}, \mathbf{M}_j \rangle| = \left(1 + o\left(\frac{\eta}{d^2}\right)\right) \left(\frac{\langle w_i^{(t)}, \mathbf{M}_j \rangle + \langle v_i^{(t)}, \mathbf{H}_j \rangle}{2}\right). \tag{165}$$

Given that $\left(1 + o\left(\frac{\eta}{d^2}\right)\right) < \left(1 + \frac{\eta}{d}\right)$, and $\frac{\langle w_i^{(t)}, \mathbf{M}_j \rangle + \langle v_i^{(t)}, \mathbf{H}_j \rangle}{2} < b_i^{(t)}$, it follows that:

$$|\langle w_i^{(t+1)}, \mathbf{M}_j \rangle| < b_i^{(t+1)}. \tag{166}$$

If $|\langle w_i^{(T_1)}, \mathbf{M}_j \rangle| < b_i^{(T_1)}$, then $|\langle w_i^{(t)}, \mathbf{M}_j \rangle| < b_i^{(t)}$ for $t \leq T_2$. Thus, with high probability, for $t \leq T_2$, we have:

$$\mathbf{1}_{\left|\left\langle w_i^{(t)}, x_p \right\rangle\right| \geq b_i^{(t)}} \cdot \mathbf{1}_{\left|\left\langle v_i^{(t)}, y_p \right\rangle\right| \geq b_i^{(t)}} = 0. \tag{167}$$

$$|\langle w_i^{(t+1)}, \mathbf{M}_j \rangle| \leq \left(1 + o\left(\frac{\eta}{d^2}\right)\right)^t \left(\frac{\langle w_i^{(T_1)}, \mathbf{M}_j \rangle + \langle v_i^{(T_1)}, \mathbf{H}_j \rangle}{2}\right) \tag{168}$$

There exists $T_2 = \Theta\left(\frac{d \log d}{\eta}\right)$ such that the following conditions hold:

$$\left(1 + \eta \frac{C_z}{d}\right)^{T_2} = \Theta(d), \tag{169}$$

indicating that $|\langle w_i^{(t+1)}, \mathbf{M}_j \rangle|$ for $i \in S_{j,\text{sure}}$ increase iteratively until:

$$\|w_i^{(T_2)}\|_2 \geq \Omega(d) \|w_i^{(T_1)}\|_2 \tag{170}$$

while, for $i \notin S_{j,\text{sure}}$, the updates diminish, such that:

$$\left(1 + o\left(\frac{\eta}{d^2}\right)\right)^{T_2} \leq 1 + o\left(\frac{1}{d}\right), \tag{171}$$

indicating negligible growth in $|\langle w_i^{(t+1)}, \mathbf{M}_j \rangle|$.

Thus we have

$$\begin{aligned} |\langle w_i^{(T_2)}, \mathbf{M}_j \rangle|^2 &= \|w_i^{(T_2)}\|_2^2 - \sum_{j \in [d], j \notin \mathcal{N}_i} \langle w_i^{(T_2)}, \mathbf{M}_j \rangle^2 - \sum_{j \in [d_1] \setminus [d]} \langle w_i^{(T_2)}, \mathbf{M}_j^{\perp} \rangle^2 \\ &\geq \|w_i^{(T_2)}\|_2^2 - (1 + o(1)) \|w_i^{(T_1)}\|_2^2 - (1 + o(1)) \|w_i^{(0)}\|_2^2 \\ &\geq (1 - o(1)) \|w_i^{(T_2)}\|_2^2. \end{aligned} \tag{172}$$

Finally, for $i \notin S_{j,\text{sure}}$, we have:

$$\|w_i^{(T_2)}, \mathbf{M}_j\|_2 \leq (1 + o(\frac{1}{d})) \cdot O\left(\frac{\|w_i^{(T_1)}\|_2}{\sqrt{d}}\right) \leq O\left(\frac{\|w_i^{(T_2)}\|_2}{\sqrt{d}}\right), \tag{173}$$

and for noise components:

$$|\langle w_i^{(T_2)}, \mathbf{M}_j^{\perp} \rangle|_2 \leq O\left(\frac{\|w_i^{(T_2)}\|_2}{\sqrt{d_1}}\right). \tag{174}$$

We summarize the results when $T_1 < t \leq T_2$ as follows:

1. For $i \in S_{j,\text{sure}}$, the alignment strength satisfies:

$$|\langle w_i^{(T_2)}, \mathbf{M}_j \rangle|^2 > (1 - o(1)) \frac{\|w_i^{(T_2)}\|_2^2 + \|v_i^{(T_2)}\|_2^2}{2} \tag{175}$$

without $j'$ that represents the corresponding spurious alignment feature.

2. For $i \notin S_{j,\text{pot}}$, the alignment strength satisfies:

$$|\langle w_i^{(T_1)}, \mathbf{M}_j \rangle|^2 \leq O(\frac{1}{d}) \cdot \frac{\|w_i^{(T_2)}\|_2^2 + \|v_i^{(T_2)}\|_2^2}{2} \tag{176}$$

3. For $\mathbf{M}_j^\perp$ where $j \in [d_1] \setminus [d]$, we have:

$$|\langle w_i^{(t+1)}, \mathbf{M}_j^\perp \rangle|^2 < O\left(\frac{1}{d_1}\right) \cdot \frac{\|w_i^{(T_2)}\|_2^2 + \|v_i^{(T_2)}\|_2^2}{2}. \tag{177}$$

Similar results also hold for $v_i$.

### I.3. Phase III Convergence of ITCP on Synthetic Data

Similarly to convergence Phase III in ITCP on Raw Data when $T_2 \leq t \leq T_3$, using Eq (24), Eq (27), and Eq (28), the loss function $L$ becomes convex with respect to $w_i$ and $v_i$ independently when $(x_p, y_p)$ and $(x_n, y_n)$ contain the true feature $j$.

We verify that the following inequality holds

$$\begin{aligned} L_j(w_i^{(t+1)}, v_i^{(t+1)}) \leq L_j(w_i^{(t)}, v_i^{(t)}) \\ + \left\langle \nabla L_j(w_i^{(t)}, v_i^{(t)}), (w_i^{(t+1)} - w_i^{(t)},\ v_i^{(t+1)} - v_i^{(t)}) \right\rangle \\ + \frac{l_{i,j}}{2} \left\| (w_i^{(t+1)} - w_i^{(t)},\ v_i^{(t+1)} - v_i^{(t)}) \right\|^2 \end{aligned} \tag{178}$$

Let $L = \max_{i \in m}(l_{i,j}/(2\tau)) = \Theta(1)$ and $\eta = \frac{1}{L}$ to ensure a monotonic decrease, plug Eq (25) and Eq (26) into Eq (178), we have

$$L_j(w_i^{(t+1)}, v_i^{(t+1)}) \leq L_j(w_i^{(t)}, v_i^{(t)}) - \frac{\eta}{2} \|\nabla L_j(w_i^{(t)}, v_i^{(t)})\|^2. \tag{179}$$

Under our data assumptions for $S_w$ and conclusion in Eq (96) , we define $w_i^* = \alpha_{i,j}^* \mathbf{M}_j, v_i^* = \alpha_{i,j}^* \mathbf{H}_j$. Thus, $L_j(w_i^*, v_i^*)$ captures both the alignment with the true feature $\mathbf{M}_j, \mathbf{H}_j$ and the spurious feature $\mathbf{M}_{j'}, \mathbf{H}_{j'}$, representing the minimal loss achievable under the influence of both true and spurious features in the optimization process. Using Eq (81), we know $w_i^{(T_2)} = \Theta(d)$, so $L_j(w_i^*, v_i^*) = -\Theta(d)$.

By the property of smoothness, we have

$$\|\nabla L_j(w_i^{(t)}, v_i^{(t)})\|_2^2 \geq \frac{2}{L} \left( L_j(w_i^{(t)}, v_i^{(t)}) - L_j(w_i^*, v_i^*) \right) \tag{180}$$

Take the telescope sum of from $T_2$ to $T_3$, we have

$$\begin{aligned} \frac{1}{T_3 - T_2} \sum_{t=T_2}^{T_3} L_j(w_i^{(t)}, v_i^{(t)}) &\leq L_j(w_i^*, v_i^*) + \frac{L^2 \Delta_0}{T_3 - T_2} \\ &\overset{\diamondsuit}{\leq} L_j(w_i^*, v_i^*) + \Theta(1) \end{aligned} \tag{181}$$

where $\Delta_0 = L_j(w_i^{(T_1)}, v_i^{(T_1)}) - L_j(w_i^*, v_i^*) = \Theta(1)$. In $\diamondsuit$, we use $T_2 = \Theta(d)$, and $L = \Theta(\frac{1}{d})$ .

Generalized to every $j \in d$, the same convergence holds for all $i \in S_{j,\text{sure}}$ when $(x_p, y_p)$ and $(x_n, y_n)$ contain feature $j, j'$. For all $(x_p, y_p)$ and $(x_n, y_n)$ in $S_w$, the following inequality holds:

$$\frac{1}{T_3 - T_2} \sum_{t=T_2}^{T_3} L(f^{(T_3)}, h^{(T_3)}) \leq L(f^*, h^*) + \Theta(1). \tag{182}$$

### I.4. Summary

ITCP trained on recaptioned data $\tilde{S}$ proceeds according to Eq. (1). After $T = \Theta(d^2 \log d)$ SGD iterations with batch size $B = \Omega(d)$ and learning rate $\eta = O(1)$, the returned weights $(\widetilde{\mathbf{W}}, \widetilde{\mathbf{V}})$ achieve a contrastive loss that is asymptotically optimal:

$$\frac{\tilde{L}(f_{\widetilde{\mathbf{W}}}, h_{\widetilde{\mathbf{V}}}) - \tilde{L}^*}{\left|\tilde{L}^*\right|} \leq o(1). \tag{183}$$

Each neuron pair $(\tilde{w}_i, \tilde{v}_i)$ in $(\widetilde{\mathbf{W}}, \widetilde{\mathbf{V}})$, for $i \in [m]$, primarily encodes a single aligned feature indexed by a set $\tilde{N}_i \subseteq [d]$, with $|\tilde{N}_i| = 1$. Specifically, we have:

$$\begin{aligned} \tilde{w}_i &= \sum_{j \in \tilde{N}_i} \tilde{\alpha}_{i,j} \mathbf{M}_j + \sum_{j \in [d] \setminus \tilde{N}_i} \tilde{\beta}_{i,j} \mathbf{M}_j + \sum_{j \in [d_1] \setminus [d]} \tilde{\gamma}_{i,j} \mathbf{M}_j^{\perp}, \\ \tilde{v}_i &= \sum_{j \in \tilde{N}_i} \tilde{\alpha}_{i,j} \mathbf{H}_j + \sum_{j \in [d] \setminus \tilde{N}_i} \tilde{\beta}_{i,j} \mathbf{H}_j + \sum_{j \in [d_1] \setminus [d]} \tilde{\gamma}_{i,j} \mathbf{H}_j^{\perp}, \end{aligned} \tag{184}$$

where $\tilde{\alpha}_{i,j}^2 = \Theta(\|\tilde{w}_i\|_2^2 + \|\tilde{v}_i\|_2^2)$, and the residual terms satisfy $\tilde{\beta}_{i,j} / \tilde{\alpha}_{i,j} \leq O(1/\sqrt{d})$, $\tilde{\gamma}_{i,j} / \tilde{\alpha}_{i,j} \leq O(1/\sqrt{d_1})$.

Moreover, for every feature index $j \in [d]$, there exists an $\Omega(1)$ many of neurons $i \in [m]$ such that $\tilde{N}_i = \{j\}$, indicating that each semantic concept is distinctly captured by dedicated neuron pairs.

## Appendix J. Downstream Task

We consider the same zero-shot classification task as in Section B.5, where the image $x$ and the class-wise text prompts $\{y_k\}_{k=1}^K$ are given. Each prompt $y_k$ corresponds to one of $K$ class labels, and the goal is to classify $x$ into the class with the best matching prompt.

Each text prompt $y_k$ is generated as:

$$y_k = \mathbf{H} z'_{y_k} + \xi_{y_k}, \quad \|z'_{y_k}\|_0 = \Theta(1), \quad \|z'_{y_k}\|_{\max} = \Theta(1). \tag{185}$$

Each test image $x$ is generated as:

$$x = \mathbf{M}' z'_x + \xi_x, \quad \|z'_x\|_0 = \Theta(1), \quad \|z'_x\|_{\max} = \Theta(1), \tag{186}$$

where $\mathbf{M}' = \mathbf{M}\mathbf{P}_1$, and

$$\max_{i,j} |(\mathbf{P}_1)_{ij} - \delta_{ij}| \leq O(1/\sqrt{d}). \tag{187}$$

If $x$ belongs to class $k$, then:

$$\left\|(z'_x)^\top z'_{y_k}\right\|_2 > \left\|(z'_x)^\top z'_{y_{k'}}\right\|_2, \quad \forall k' \neq k. \tag{188}$$

Using Eq. (96) and Eq. (144), let $f(x)$ and $h(y)$ represent the image encoder and text encoder of ITCP on raw data, respectively. Given a data sample $x$ containing $\mathbf{M}_j$ and $y$ containing $\mathbf{H}_{j'}$, where $j'$ is the spurious feature corresponding to $j$, it holds with high probability that:

$$\left\langle \frac{f(x)}{\|f(x)\|_2}, \frac{h(y)}{\|h(y)\|_2} \right\rangle = \Theta(1). \tag{189}$$

This result implies that the image and text encoders of ITCP on raw data struggle to distinguish between features $j$ and $j'$, leading to misclassification caused by spurious correlations.

However, using Eq. (175) and Eq. (176), let $\tilde{f}(x)$ and $\tilde{g}(y_k)$ denote the image and text encoders of ITCP on recaptioned data. Given $x$ containing $\mathbf{M}_j$ and $y$ containing spurious $\mathbf{H}_{j'}$, it holds with high probability $1 - \Theta\left(\frac{1}{d}\right)$ that:

$$\left\langle \frac{\tilde{f}(x)}{\|\tilde{f}(x)\|_2}, \frac{\tilde{g}(y)}{\|\tilde{g}(y)\|_2} \right\rangle \leq \Theta\left(\frac{1}{d}\right). \tag{190}$$

This result implies that the image and text encoders of ITCP on synthetic data are capable of effectively distinguishing the true feature from the spurious feature.

Because $K = \Theta(1)$ and $\|z_{y_k}\|_0 = \Theta(1)$, we only have constant class classification and constant features in images. Thus, we have:

1. For the image encoder $f(x)$ and text encoder $h(y_k)$ of ITCP on raw data:

$$\Pr\left(\arg\max_k \langle f(x), h(y_k)\rangle = k_x\right) = 1 - \Theta(1), \tag{191}$$

2. For the image encoder $\tilde{f}(x)$ and text encoder $\tilde{g}(y_k)$ of ITCP on synthetic data:

$$\Pr\left(\arg\max_k \langle \tilde{f}(x), \tilde{g}(y_k)\rangle = k_x\right) = 1 - o(1). \tag{192}$$